



**CORROSION PROPERTIES OF AGED AZ31 MG
ALLOY CONTAINING ND AND LA**

**2023
MASTER THESIS
METALLURGICAL AND MATERIALS
ENGINEERING**

Sarah Khazaal Jabbar MADHI

**Thesis Advisor
Assist.Prof.Dr. İsmail Hakkı KARA**

**CORROSION PROPERTIES OF AGED AZ31 MG ALLOY CONTAINING
ND AND LA**

Sarah Khazaal Jabbar MADHI

T.C.

Karabuk University

Institute of Graduate Programs

Department of Metallurgical and Materials Engineering

Prepared as

Master Thesis

Thesis Advisor

Assist.Prof.Dr. İsmail Hakkı KARA

**KARABÜK
August 2023**

I certify that in my opinion the thesis submitted by Sarah Khazaal Jabbar MADHI titled “CORROSION PROPERTIES OF AGED AZ31 MG ALLOY CONTAINING ND AND LA” is fully adequate in scope and in quality as a thesis for the degree of Master of Science

Assist. Prof. Dr. İsmail Hakkı KARA
Thesis Advisor, Department of Metallurgical and Materials Engineering

This thesis is accepted by the examining committee with a unanimous vote in the Department of Metallurgical and Materials Engineering as a Master of Science thesis.
August 10, 2023

<u>Examining Committee Members</u> (Institutions)	Signature
Chairman: Prof. Dr. Hayrettin AHLATCI (KBU)
Member : Prof. Dr. Mustafa ACARER (SU)
Member : Assist. Prof. Dr. İsmail Hakkı KARA (KBU)

The degree of Master of Science by the thesis submitted is approved by the Administrative Board of the Institute of Graduate Programs, Karabuk University.

Assoc. Prof. Dr. Zeynep ÖZCAN
Director of the Institute of Graduate Programs

“I declare that all the information within this thesis has been gathered and presented in accordance with academic regulations and ethical principles and I have according to the requirements of these regulations and principles cited all those which do not originate in this work as well.”

Sarah Khazaal Jabbar MADHI

ABSTRACT

Master Thesis

CORROSION PROPERTIES OF AGED AZ31 MG ALLOY CONTAINING ND AND LA

Sarah Khazaal Jabbar MADHI

Karabük University

Institute of Graduate Programs

The Department of Metallurgical and Materials Engineering

Thesis Advisors:

Assist.Prof.Dr. İsmail Hakkı KARA

August 2023, 81 pages

Investigation of the effects of heat treatment and alloy modifications on the corrosion behavior and microstructural properties of AZ31 magnesium alloys. The study focuses on AZ31 alloys subjected to low-pressure chill casting with the addition of La and Nd elements. Corrosion evaluations were performed using potentiodynamic corrosion tests and immersion tests in saline and biological environments. The microstructures were analyzed by optical microscopy (OM) and scanning electron microscopy (SEM), with the elemental composition determined by energy dispersive X-ray spectroscopy (EDX). Wear tests were also conducted to assess the performance of the alloys in different media. The results show that the corrosion behavior of the alloy compositions (e.g. AZ31-0.5Nd-0.1La-20 min and AZ31-0.5Nd-0.5La-20 min) increases in corrosion behavior when exposed to saline and biological environments, respectively have maximum corrosion rates. Corrosion rates were affected by alloy composition

and exposure time. The results of the immersion test show that AZ31-10min showed the highest weight loss while AZ31-0.5Nd-0.5La-3h showed the lowest weight loss during the immersion test. The mass loss decreased over time due to the accumulation of salts and dissolved elements on the sample surfaces. Optical micrographs showed the presence of crystal boundaries and twinning in certain coarse grains of alloys containing 0.5% Nd and %La. Grain size was affected by heat treatment, resulting in larger grains due to slow cooling. Aluminum, zinc, and manganese grains showed semicircular shapes, while additions of La and Nd manifested as short fibers. EDX analysis provided insight into the elemental composition of each alloy. Wear rates have been evaluated in both biological and arid environments. In particular, AZ31-0.5Nd-0.1La-1h showed the highest wear rate in biological media, while AZ31-0.5Nd-0.2La-2h showed the highest wear rate under dry conditions.

Key Word : AZ31 alloy, Heat treatment, Casting, Electrochemical corrosion
, Wear

Science Code : 91518

ÖZET

Yüksek Lisans Tezi

ND VE LA İÇEREN YAŞLANDIRILMIŞ AZ31 MG ALAŞIMININ KOROZYON ÖZELLİKLERİ

Sarah Khazaal Jabbar MADHI

Karabük Üniversitesi

Fen Bilimleri Enstitüsü

Metalurji ve Malzeme Mühendisliği

Tez Danışmanı:

Dr. Öğr. Üyesi İsmail Hakkı KARA

Ağustos 2023, 81 sayfa

Isıl işlem ve alaşım modifikasyonlarının AZ31 magnezyum alaşımlarının korozyon davranışı ve mikroyapısal özellikleri üzerindeki etkilerinin incelenmesi. Çalışma, La ve Nd elementlerinin ilavesiyle düşük basınçlı soğuk döküme tabi tutulan AZ31 alaşımlarına odaklanmaktadır. Korozyon değerlendirmeleri, tuzlu ve biyolojik ortamlarda potansiyodinamik korozyon testleri ve daldırma testleri kullanılarak gerçekleştirilmiştir. Mikroyapılar, optik mikroskopi (OM) ve taramalı elektron mikroskobu (SEM) ile analiz edildi ve temel bileşim, enerji dağılımlı X-ışını spektroskopisi (EDX) ile belirlendi. Alaşımların farklı ortamlardaki performansını değerlendirmek için aşınma testleri de yapılmıştır. Sonuçlar, alaşım bileşimlerinin (örneğin AZ31-0.5Nd-0.1La-20 min ve AZ31-0.5Nd-0.5La-20 min) korozyon davranışının sırasıyla tuzlu ve biyolojik ortamlara maruz kaldığında arttığını göstermektedir. korozyon oranları. Korozyon oranları, alaşım bileşimi ve maruz kalma

süresinden etkilenmiştir. Daldırma testinin sonuçları, AZ31-10min'in en yüksek ağırlık kaybını gösterdiğini, AZ31-0.5Nd-0.5La-3h'nin daldırma testi sırasında en düşük ağırlık kaybını gösterdiğini göstermektedir. Numune yüzeylerinde tuzların ve çözülmüş elementlerin birikmesi nedeniyle kütle kaybı zamanla azaldı. Optik mikrograflar, %0.5 Nd ve %La içeren bazı kaba alaşım tanelerinde kristal sınırlarının ve ikizlenmenin varlığını gösterdi. Tane boyutu, ısıtılardan etkilendi ve yavaş soğutma nedeniyle daha büyük taneler elde edildi. Alüminyum, çinko ve manganez taneleri yarım daire şekiller gösterirken, La ve Nd ilaveleri kısa lifler olarak kendini gösterdi. EDX analizi, her bir alaşımın temel bileşimi hakkında fikir verdi. Aşınma oranları hem biyolojik hem de kurak ortamlarda değerlendirilmiştir. Özellikle AZ31-0.5Nd-0.1La-1h biyolojik ortamda en yüksek aşınma oranını gösterirken AZ31-0.5Nd-0.2La-2h kuru koşullarda en yüksek aşınma oranını göstermiştir.

Anahtar Sözcükler : AZ31 alaşımı, Isıl işlem, Döküm, Elektrokimyasal korozyon, Aşınma.

Bilim Kodu : 91518

ACKNOWLEDGMENT

First of all, profusely all thanks be for ALLAH who enable me to achieve this work.

I would like to express my gratitude to my supervisor, Dr. Öğr. Üyesi İsmail Hakkı KARA for his enthusiasm and support. His suggestions, guidance and moral support in difficult times have been essential for completing this work.

In advance, I would like to thank the examining committee members for being willing to collaborate decisively with this work.

To the one who honored me with bearing his name, my father, may God Almighty have mercy on him.... who spent the precious and precious things in order for me to reach a high academic degree and left before seeing the fruit of his planting....

To the light of my eyes, the light of my path, and the joy of my life, my mother, ...whose prayers and words were the companion of brilliance and excellence...

To a light that illuminates my darkness when days and circumstances turn me off. To a cloud that shelters me and waters me without wanting to return its favor.. To the hands that extend help to me when I stumble To the support of my faithful husband (Muhannad)

To my dear uncle and dear aunt (Dr. Tariq and Suzanne), thank you for standing and supporting me throughout these years.

To the seed of the heart and hope for tomorrow, my beloved children (Tim and Karam)

To my brother and sisters (Ahmed, Rana, Rasha, Hala), I give you the gift of love, honor and dignity.

To my friends and to everyone who taught me a letter and supported me even with a smile

CONTENTS

	<u>Page</u>
APPROVAL.....	ii
ABSTRACT.....	iv
ÖZET.....	vi
ACKNOWLEDGMENT.....	viii
CONTENTS.....	ix
LIST OF FIGURES	xii
LIST OF TABLES	xiv
SYMBOLS AND ABBREVIATIONS INDEX	xv
PART 1	1
INTRODUCTION	1
PART 2	7
THEORETICAL BACKGROUND.....	7
2.1. BIOMATERIALS	7
2.2. MAGNESIUM AND ITS ALLOYS AS BIOMATERIALS	10
2.3. CLASSIFICATION OF MAGNESIUM ALLOYS	13
2.4. ALLOYING ELEMENTS	17
2.4.1. Aluminum (Al)	17
2.4.2. Tin (Sn).....	18
2.4.3. Zinc (Zn).....	19
2.4.4. Manganese (Mn).....	20
2.4.5. Gadolinium (Gd).....	21
2.4.6. Lanthanum (La)	21
2.5. AZ31 ALLOY	22
2.6. BIODEGRADATION AND CONTROL OF Mg ALLOY	23
2.7. BIOCOMPATIBILITY OF Mg ALLOY.....	26
2.8. ELECTROCHEMICAL CORROSION	27

2.8.1. Types of Corrosion	28
2.8.2. Corrosion of Magnesium and Magnesium Alloys.....	30
2.8.3. Tribocorrosion of Mg Alloys.....	33
2.9. THE HEAT TREATMENT OF Mg AND IT'S ALLOY	35
2.10. APPLICATION OF MAGNESIUM ALLOYS	36
PART 3	37
MATERIALS AND METHOD	37
3.1. MATERIALS	37
3.2. PREPRATION OF SAMPLES TO TEST	39
3.2.1. Material Cutting.....	39
3.2.2. Cold Bakelite	40
3.3. HEAT TREATMENT	41
3.4. MICROSTRUCTURE CHARACTERIZATION	41
3.4.1. Microstructure.....	41
3.4.2. Physical Properties.....	43
3.4.3. Immersion Corrosion Test	44
3.4.4. Potentiodynamic Polarization Test.....	45
3.4.5. Wear Test	46
PART 4	47
RESULT AND DISSCSUION	47
4.1. INTRODUCTION.....	47
4.2. MICROSTRUCTURE CHARACTERIZATION	47
4.2.1. Optical Microstructure (OM) Analysis.....	47
4.2.2. SEM analysis of Alloys	52
4.3. PHYSICAL PROPERTIES	57
4.4. WEAR TEST.....	59
4.5. ELECRTOCHEMICAL ANALYSIS	62
4.5.1. Immersion Corrosion Test Results	62

4.5.2. Potentiodynamic Polarization Corrosion Test Results	63
PART 5	72
CONCLUSIONS	72
REFERENCES.....	73
RESUME	81

LIST OF FIGURES

	Page
Figure 1.1. Magnesium and its alloying	2
Figure 1.2. The effect of alloying elements on the corrosion behavior of magnesium	4
Figure 2.1. Metallic biomaterials used in the body	10
Figure 2.2. The unit cell, major planes and directions for the element magnesium... ..	10
Figure 2.3. Mg-Sn secondary phase diagram	18
Figure 2.4. Mg-Zn secondary phase diagram	19
Figure 2.5. Mg-Mn secondary phase diagram	20
Figure 2.6. Mg-Gd secondary phase diagram.....	21
Figure 2.7. Mg-La secondary phase diagram	22
Figure 2.8. Mg-Al phase diagram.....	23
Figure 2.9. Possible interactions between any Mg alloy and a biological environment.....	25
Figure 2.10. Pit corrosion of Mg alloys	28
Figure 2.11. (IGC) of Mg alloys	29
Figure 2.12. Galvanic corrosion of Mg alloys	30
Figure 2.13. Pourbaix diagram of pure Mg element	31
Figure 2.14. The anodic and cathodic reactions for the element magnesium	32
Figure 2.15. Four basic parameters affecting the tribocorrosion mechanism	33
Figure 3.1. Low pressure permanent mold casting furnace.....	37
Figure 3.2. Experimental program of the present study.	39
Figure 3.3. Cutting device used in the study.	40
Figure 3.4. The cold bakelite mold used in the study.....	40
Figure 3.5. Heat treatment furnace used in the study.	41
Figure 3.6. OM device used in the study.....	42
Figure 3.7. Carl Zeiss ultra plus gemini FESEM	42
Figure 3.8. PRECISE XB 220A precision balance used in the experiments.....	43
Figure 3.9. Immersion test of AZ31 alloys.....	44
Figure 3.10. Potentiodynamic device used in the study.....	45
Figure 3.11. Schematic representation of the wear test.	46

Figure 4.1. AZ3110 MIN.	54
Figure 4.2. AZ31 1 hour.....	54
Figure 4.3. NO 2 30 min.	55
Figure 4.4. NO 2 1 hour.....	55
Figure 4.5. NO 3 10 min.....	55
Figure 4.6. NO 3 2 hour.....	56
Figure 4.7. NO 4 20 min.....	56
Figure 4.8. NO 4 3 hour.....	56
Figure 4.9. Wear diagram of AZ31.	59
Figure 4.10. Wear diagram of AZ31-0.5Nd-0.1 La	60
Figure 4.11. Wear diagram of AZ31-0.5Nd-0.2La.	60
Figure 4.12. Wear diagram of AZ31-0.5Nd-0.4 La.	61
Figure 4.13. Corrosion immersion test diagram for AZ31 samples.....	63
Figure 4.14. Potentiodynamic diagram for AZ31 samples in saline solution.....	64
Figure 4.15. Potentiodynamic diagram for AZ31-0.5Nd-0.1 La samples in saline solution.....	64
Figure 4.16. Potentiodynamic diagram for AZ31-0.5Nd-0.2 La samples in saline solution.....	65
Figure 4.17. Potentiodynamic diagram for AZ31-0.5Nd-0.5 La samples in saline solution.....	65
Figure 4.18. Potentiodynamic diagram of AZ31 samples in SBF.	68
Figure 4.19. Potentiodynamic diagram of AZ31-0.5Nd-0.1 La samples in SBF.	68
Figure 4.20. Potentiodynamic diagram of AZ31-0.5Nd-0.2 La samples in SBF.	68
Figure 4.21. Potentiodynamic diagram of AZ31-0.5Nd-0.5 La samples in SBF.	69

LIST OF TABLES

	<u>Page</u>
Table 2.1. Mechanical properties of some biomaterials	12
Table 2.2. Main alloying elements	13
Table 2.3. Common magnesium alloys and their applications.	16
Table 3.1. Casting conditions.....	38
Table 3.2. Alloying elements used in the study	38
Table 4.1. Optical micrographs of AZ31	48
Table 4.2. SEM and EDX of the prepared AZ31 alloy	52
Table 4.3. Density for the prepared alloy	58
Table 4.4. I_{corr} and E_{corr} rates for the corrosion test of the AZ31	65
Table 4.5. I_{corr} and E_{corr} rates for the corrosion test of the AZ31 with SBF	70

SYMBOLS AND ABBREVIATIONS INDEX

SYMBOLS

I_{corr} : Corrosion current density

E_{corr} : corrosion potential

MPa : Megapascal

E : Young's modulus

μm : Micrometer

°C : Degrees Celsius

ABBREVIATIONS

SEM : Scanning Electron Microscope

ASTM : American Society for Testing and Materials

SBF : Simulated Body Fluid

ISO : International Organization For Standardization

EDS : Energy-Dispersive Spectrometry

SCE : Saturated Calomel Electrode

C₂O : carbon monoxide

PART 1

INTRODUCTION

1.1 INTRODUCTION

The biomechanical function of living metabolism depends on the harmonious functioning of the bone and muscle system. Weakening/degeneration of bone and muscle tissue as a result of genetic or subsequent damage/diseases disrupts this biomechanical order. In cases where surgical interventions are necessary to restore biomechanical function, the implantation process and the type of medical instruments are of great importance. In this context, innovative moves that will increase patient comfort, accelerate post-implantation recovery time and minimize the need for surgical intervention have been the subject of many studies in the literature [1]. Studies on Magnesium (Mg) alloys, which have recently been widely used in the field of biomaterials, are also within this research area. The metallic implant group, which is used to eliminate orthopedic problems that require surgical intervention, has very important functions and can be used directly in place of the damaged or lost bone structure of the patient, or they can be implanted as a reinforcement element. They are produced in different designs and types to be widely used in many different anatomical regions such as bone nails, bone plates, spinal systems, and mini plates. With the developing technology, a wide variety of metals are made usable in the biomedical field with different surface modification techniques. In line with these possibilities, metallic implants can be classified under two types as bio-inert and biodegradable in the most general sense. Material groups with bio-inert properties are generally preferred for the implantation of an orthopedically traumatized bone [2]. Metallic materials containing Titanium (Ti) and its alloys and Cobalt Chromium (CoCr) are frequently used in such applications [3]. The high success of these materials in bone stabilization, the need for long-term healing time, and the fact that they can be used instead of bone in some cases are the most

important reasons for preference [4]. However, the success of implantation decreases in some interventions as a result of some disadvantages as well as the reasons for the preference of the materials in the bio-inert group [5]. At this point, the preference of biodegradable species such as Mg and its alloys makes a significant contribution to implant and healing performance. Most often, types modified by the reinforcement of alloying elements are used Figure 1.

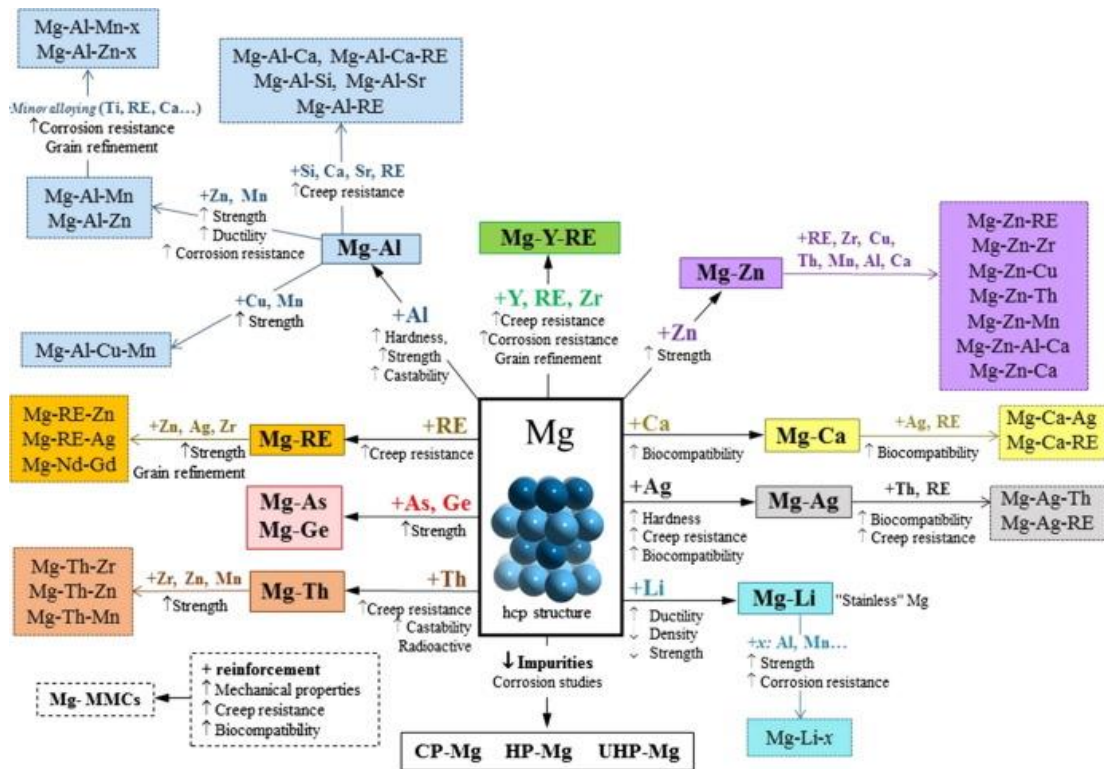


Figure 1.1. Magnesium and its alloying [6].

It was used especially as a building material for airplanes in World War I and II. Mg alloys, which continued their attraction in the World War II, left their place to aluminum alloys in the following periods due to reasons such as low amount of ore and production cost. However, recently, the use of Mg alloys has been brought to the agenda again due to increasing CO2 emission and decreasing energy efficiency, lightness and special strength. Mg alloys, which are mainly used in the automotive sector and aviation applications, are used even in the cases of devices such as mobile phones and laptops, which are indispensable in our daily lives. The product range of High Mg alloys covers a wide area. However, it is of great importance to develop Mg

alloys, which have poor formability at room temperature due to the HCP structure, and to reduce production costs. In recent years, alloying has created a wide field of study for the production of Mg alloys with good deformability and mechanical properties at low temperatures. The texture weakening effect of elements such as Gadolinium, Yttrium and Neodymium, which are known as rare earth elements, has been determined in pure Mg and it has been provided to shape more easily. Gd, Nd and Ce were used to improve the rolling capability of the AZ31 Mg alloy, which is the most widely used in the AZ series, and positive results were obtained.

Mg and its alloys have become a frequently preferred material group, especially in fracture treatments, due to their similar characteristics to the mechanical properties of bone (Witte et al. 2005). When exposed to biological fluids in living metabolism, Mg shows biodegradable properties and can be completely dissolved within the required time. Magnesium is the fourth most abundant cation in human metabolism and is a natural mineral found in bone. Therefore, the products resulting from the degradation of Mg-based implants can be excreted harmlessly in the urine [7]. However, this degradation is a major problem in many engineering applications, as it usually proceeds rapidly and uncontrollably. By controlling the rate of degradation, the functionality of the implant can be preserved within the healing period of the bone. Considering that decomposition progresses as a corrosion mechanism, all modifications that will increase corrosion resistance on the material surface reduce the problems at this point. The alloying elements that affect the corrosion rate are given in Figure 2 [8].

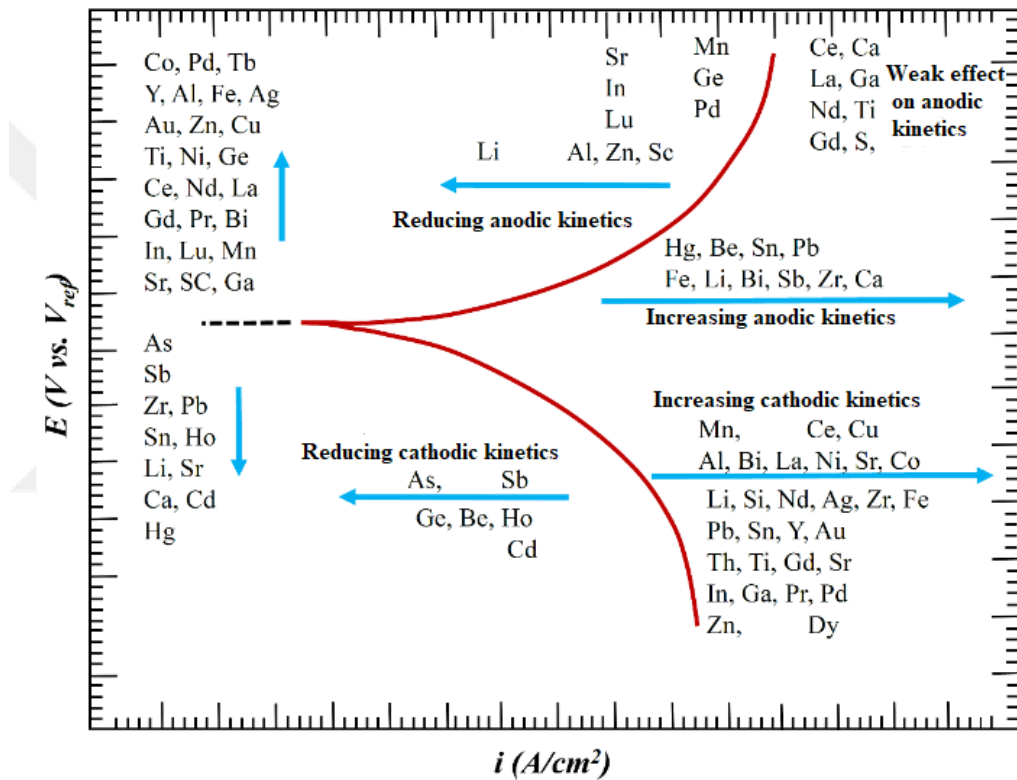


Figure 1.2. The effect of alloying elements on the corrosion behavior of magnesium [9].

rapid and uncontrolled degradation may cause many harmful effects on living metabolism [8]. These effects usually occur as a result of the rapid mixing of Mg ions into living tissues and body fluids. The Mg ion release rate is directly proportional to the corrosion rate of the surface. Therefore, there are many studies in the literature on increasing the corrosion resistance of Mg and its alloys [10]. The diversity and concentration of ions in very different numbers and amounts in living tissue increase the corrosive effects on the implant. This situation creates the need to analyze the corrosion behavior of the metal preferred as the implant material in a wide range. In this context, when we look at the studies in the literature; metal-oxide, metal-nitride derivative ceramic coatings and organic coatings are applied and the effect of Mg alloys on corrosion resistance is examined [11].

In the perspective of in vitro environment; Testing, taking into account the mechanisms of wear, corrosion and tribocorrosion, provides a fairly large pool of data about a biodegradable material. The diversity of the test medium (liquid) is also of

great importance with the application of these three basic mechanisms in the idea of imitating living metabolism, which forms the basis of in vitro studies (Mei et al. 2020). The element content and balance of the test solutions are more effective on metals with weak corrosion resistance such as magnesium. Tests with electrolytes with a high aggression threshold and inorganic salt content similar to living organisms have been frequently used in studies in the literature since they provide rapid degradation data in a short time. Therefore, some studies in the literature were prepared with the idea of imitating body fluid in vitro and focused on the effect of the environment. Dong et al. investigated the biodegradability behavior of Mg, Zn and Fe elements in SBF (Simulated body fluid) and DMEM (Dulbecco's Modified Eagle's Medium) solution. According to the test results, it has been determined that the SBF solution has a more aggressive effect than DMEM in the long-term test period and has a greater effect on the degradation rate [12].

In general, when the current literature is examined, studies on the use of Mg and its alloys as biomaterials have increased and it has been tried to be developed with certain surface modifications as an alternative to bio-inert materials. The processes carried out in this context include suitable coating methods applied to Mg and its alloys. Since it is working with biodegradable material group, characterization tests suitable for bio-inert material are applied. However, research on specific materials is still very limited for Mg alloys. Due to the thermochemical properties of the Mg element, the limitations on the coating processes are one of the important reasons for this situation. In addition, the fact that the mechanical properties of Mg and its alloys are quite low compared to Ti and its alloys poses a serious problem in terms of being an alternative. However, it should not be forgotten that Mg and its alloys are in the category of temporary implants or biodegradable implants, especially considering the time parameter in the field of orthopedics. Studies have shown that this distinction is rarely clearly demonstrated. Therefore, the test methods chosen should be separate from bio-inert materials. It has been observed that this profound difference is not clearly applied in the literature. In addition, ceramic and derivative coatings for Mg alloys must be shifted to applications in the biomedical field. It is seen that such modifications are mostly developed for use in the automotive and space industry. Although the existence of studies involving wear and corrosion tests is palpable in the literature, studies in the field of tribocorrosion are very few. In particular, the number of studies on an alloy such as AZ31, which is very

suitable for use in the biomedical field, has remained surprisingly low. As with pure Mg alloy, the difficulty of ceramic coatings with high wear resistance and the adhesion problem of the coating may be the main reasons for this situation. Similarly, scientific publications that evaluate three basic parameters effective in biodegradability studies together with different environments are in a very small group among studies in this field.

1.2 . OBJECTIVE OF THE WORK

The thesis aims to investigate the effect of heat treatment on the microstructure , corrosion and wear resistance of AZ31 alloys. The 5005 Al alloy is a widely used aluminum alloy that is known for its excellent corrosion resistance and moderate strength. Heat treatment is a common technique used to improve the mechanical properties of aluminum alloys by altering their microstructure.

The research will involve conducting a series of experiments on samples of AZ31 alloy to determine how different heat treatment conditions affect the microstructure , corrosion and wear resistance of the alloy.

The heat treatment process will involve heating the alloy to a specific temperature and holding it at that temperature for a predetermined amount of time before cooling it down. Different heat treatment conditions will be tested to determine the optimal treatment for improving the microstructure , corrosion and wear resistance of the alloy. The following steps can summarize this aim:

The aim of this study is primarily to produce AZ31 Mg alloys containing La, Nd and Gd by low pressure casting method. Afterwards, the rolling of the alloys produced using different rolling parameters is to produce materials with weaker texture, that is, easier to shape, higher strength and better corrosion resistance and wear behavior than the sheet AZ31 Mg alloy.

- Produce AZ31 Mg alloys containing La, Nd and Gd by casting method
- Study the microstructure changes, the microstructure , corrosion and wear resistance as a function of the heat treatment.

PART 2

THEORETICAL BACKGROUND

2.1 BIOMATERIALS

Biomaterials and medical devices are mostly used in cardiovascular, orthopedics, dental, eye, reconstructive surgery and other surgical sutures, bioadhesives. Thanks to the development of these devices from past to present, the lives of millions of living things have been saved and the quality of life has been increased. The first medical devices that were scientifically accepted in the medical field and that could be used for human health emerged at the end of the 1940s. The rising standard of living, aging population and technological developments in developing countries have ensured that the growth in this area is permanent. Studies on patient diagnosis and treatment play a leading role in biomaterials science. In order for the manufactured implant or device to become clinically meaningful;

- In vitro and in vivo tests
- Clinical trials
- Commercial and environmental permits are required [13]. Biomaterials science alone cannot support a research model. Bioinformatics, synthetic biology, computational biology, nanobiology, systems biology and other prominent fields contribute to the biomaterials discipline in the medical device and implant manufacturing process. Studies on biomaterials are carried out by using basic sciences such as cell biology, chemistry, materials science and engineering together. Therefore, knowledge and experimental activities of the above-mentioned disciplines are used in the definition, production and classification of this group of materials. In addition, the experience and suggestion of the implantation team (such as a doctor, physiotherapist) contribute to the development of biomaterials.

Biomaterials in the most general sense; It is a material group that serves the health of living things, is biocompatible, biodegradable according to needs, has the necessary chemical and mechanical properties and has the appropriate surface morphology. The material used in the manufactured medical device and/or implant varies according to its location in the body and the purpose of its operation. The ideal biomaterial is the most resistant to mechanical and chemical effects inside or outside the body. Medical problems such as inflammation, toxic reaction, allergic symptoms determine the chemical characteristics of biomaterials. The physical property of a biomaterial can be evaluated by cell interaction. Adhesion and proliferation of the cell on the material can only be achieved by providing some surface properties. Wettability, roughness, hardness and chemical composition affect adhesion [14]. The hydrophilic or hydrophobic nature of the surface determines the type of interaction between the solid implant surface and the liquid tissue. The effect of cell and bacterial adhesion, protein adsorption and platelet adhesion are important parameters. Protein adsorption of hydrophobic surfaces is less than hydrophilic surfaces. The water repellency of hydrophobic surfaces prevents the dissolution forces that may occur on the surface. Therefore, the adsorption decreases. Another important surface property is roughness. Roughness plays an important role in terms of cell adhesion and behavior on the biomaterial surface. Since flatter surfaces will create different contact angles, it affects the connections of cells or molecules on the surface.

Thus, differences in structure and function arise. For implants where low friction surfaces are desired, mirror-like smooth surfaces are sought. However, where a strong tissue-implant interaction is desired, much rougher surfaces are desired. To know the chemical properties and composition as well as the physical properties of the biomaterial surface; It determines what type of cellular bonding will occur on the surface, chemical stabilization and reactivity. The biggest effect of environmental conditions on biomaterial is corrosion. The chemical stability of the material affects its corrosion resistance and therefore its biocompatibility. Particles formed after corrosion may damage the implant surface and its surroundings. These particles disrupt the physiological nature of the body fluids in their normal balance and poison the body. Swelling occurs around the corroded implant and pain may develop. Corrosion destroys not only the chemical stability but also the mechanical integrity of the

material and causes premature fatigue damage [15]. As a result, the biodegradation time of the biomaterial is also shortened. Surface functionality is impaired. For biomaterials, in addition to physical and chemical properties, some specific material information may need to be determined. Through this information, the specific behavior of the biomaterial is characterized. Material selection is made for a specific biomechanical application by using values such as modulus of elasticity, tensile strength, yield strength, fatigue and wear properties. Biomaterials close to the Elasticity module of the bone are always the primary choice in terms of mechanics. The implant with high yield and compression strength values provides functional stability. These values should also be kept at optimum. Otherwise, brittle materials are preferred. Brittle materials also have a very high risk of sudden damage. In addition, ductile material is essential for the production of implants with complex geometries with certain strength values. An implant is not always subject to static loads. In fact, dynamic loads often force the material. Under cyclic load, cracks occur, followed by fatigue damage. This type of damage is usually seen in orthopedic implants. Longer life systems are designed by choosing materials from polyurethane, polyester and metal groups. Wear, on the other hand, occurs as a result of the relative movement of two surfaces in contact with each other and causes losses on the material surface. In some cases, damage may result from wear and fatigue. For example; This type of damage often occurs on the moving surfaces of biomaterials used in hip prostheses. In addition, other physiological factors may increase the risk of this damage [16].

Biomaterials can be examined in four different groups according to the type of material they are produced, as metallic, ceramic, polymeric and composite biomaterials. Among these groups, metallic biomaterials are the most preferred group in terms of physical, chemical and mechanical properties . In addition, easy production and low cost are other reasons for preference . The properties of a metallic biomaterial that can function without losing its properties for a desired period of time can be listed as follows [17]:

- i. Excellent biocompatibility
- ii. Appropriate mechanical properties
- iii. High corrosion resistance
- iv. High wear resistance

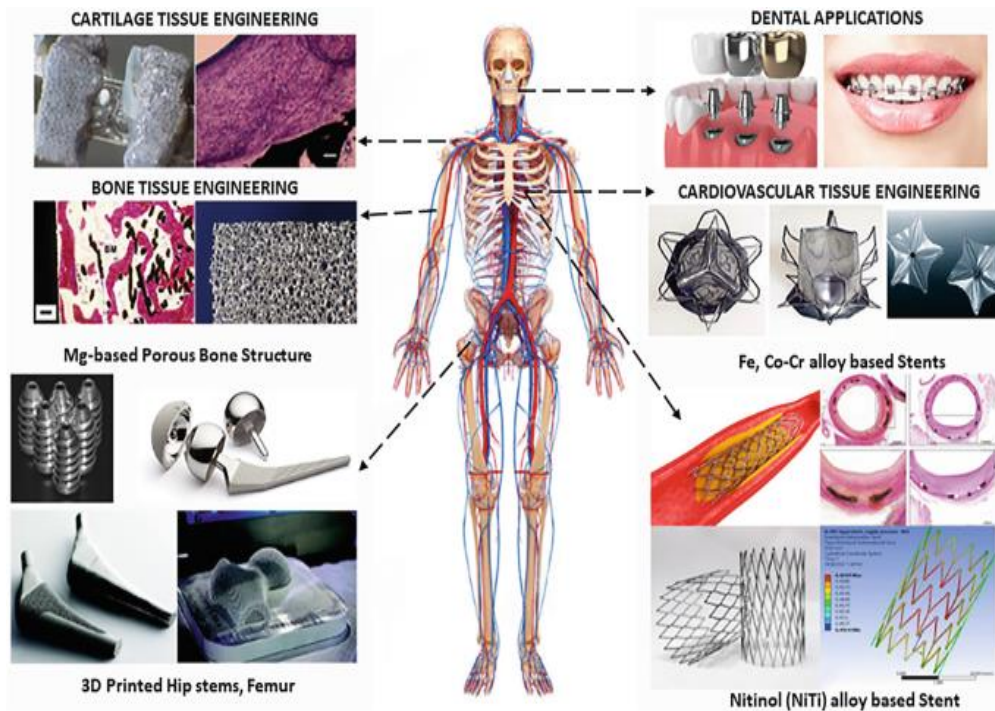


Figure 2.1. Metallic biomaterials used in the body [18].

2.2 MAGNESIUM AND ITS ALLOYS AS BIOMATERIALS

The element magnesium was discovered by Sir Humphrey in 1808. It is an alkali metal and is in group 2A in the periodic table. It has a tight-packed hexagonal (Figure 2.2) structure at room temperature [19].

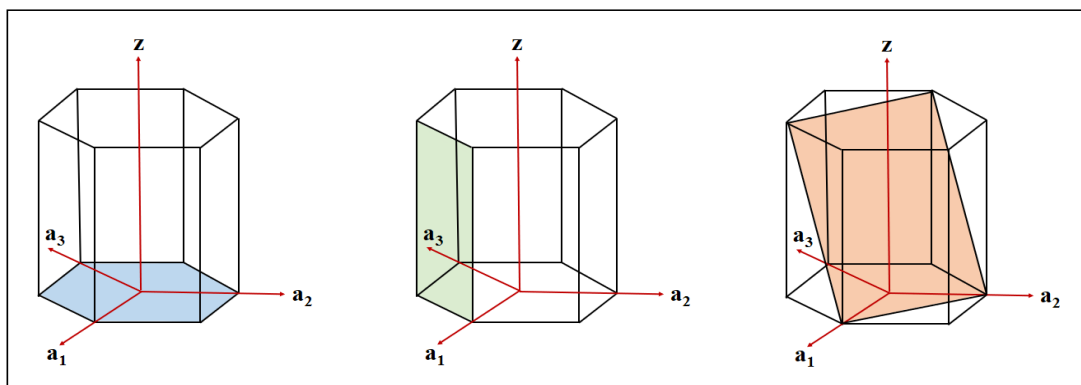


Figure 2.2. The unit cell, major planes and directions for the element magnesium [19].

Magnesium and its alloys (first Mg wires) have been used as biomaterials since 1878 . Orthopedic implants and stents are the most common types of use [5] .It is quite suitable for orthopedic implant group in terms of biodegradation and mechanical relationship. It can be an alternative to metals that are mechanically incompatible with bone tissue in areas where long-term permanent connection is desired . An implant material is subjected to many tests to measure its biological and mechanical performance. These tests are performed in vivo and in vitro. Although in vivo measurements give results very close to the performance in real use, it consists of a series of procedures that are more costly and time-consuming than in vitro tests. Therefore, in vitro tests performed under the right optimized experimental conditions play a major role in the characterization of Mg and its alloys as biomaterials. Its in vitro characterization is examined under two main headings (bio-corrosion/biodegradation, toxicity/biocompatibility) [20] . Mg and its alloys differ from other biomaterials in terms of physical and mechanical similarity to human bone . The fact that the density and modulus of elasticity of magnesium is very close to the bone eliminates the elastic incompatibility between implant/bone . In addition, there is Mg in the natural structure of the bone and it is one of the metals necessary for metabolism. Mg and its alloys are highly soluble by the body. Being one of the main metals naturally found in the body, compatible with bone and biodegradability, and sufficient mechanical properties, it has recently enabled it to be used as a biomaterial. Magnesium-based biodegradable alloys generally consist of four groups. These; pure Mg, alloys containing Al (AZ31, AZ91, LAE422, AM60), rare earth elements (such as AE21, WE 43) and alloys without Al (such as WE43, MgCa0,8, MgZn6). In order to gain the physical and mechanical properties necessary for the use of these alloys in the orthopedic field; a) Grain size is optimized, b) Corrosion resistance is increased, c) Strength is increased with intermetallic formations, d) Coating process is applied [21].

Table 2.1. Mechanical properties of some biomaterials [22].

Alloy	Symbol	Density (g/cm³)	Yield Strength (MPa)	Tensile Strength (MPa)	Modulus of Elasticity (GPa)
Bone		1,8 – 2,1	104 – 121	110 – 130	15 - 25
Mg and alloy	Pure Mg	1,74 – 2	65 – 100	90 – 190	41 – 45
	AZ31	1,78	185	263	45
	AZ91	1,81	160	150	45
	WE43	1,84	170	220	44,2
Fe and Mn alloys	Fe ₂₀ Mn	7,73	420	700	207
	Fe ₃₅ Mn	-	230	430	-
Zn-based alloys	Zn-Al-Cu	5,79	171	210	90
Stainless steel	SS316L	7,9	190	490	200
Ti-and alloys	Ti ₆ Al ₄ V	4,43	880	950	113,8
	Ti ₆ Al ₇ Nb	4,52	800	900	105
Co-Cr alloy	CoCr ₂₀ Ni ₁₅ Mo ₇	7,8	240 - 250	450 - 960	195 - 230
Bioceramic	Alumina	4	-	400 – 580	260 – 410
Natural and synthetic polyesters	Collage	-	-	2,6 – 605	5 – 11,5
	PLGA	1,30 –	3,8 –	13,9 –	1,69
	PCL	1,34	26,6	16,7	281 -
		1,145	8,37 –	68,45 –	686
			14,66	102,7	

Today, the most studied Mg alloys are commercial alloys developed for the transportation industry as implant material [23]. The designation system for Mg alloys generally follows the American Society for Testing and Materials (ASTM) nomenclature [24] and uses a typical letter-figure combination. Mg alloys can be divided into three main groups: pure Mg (Mg) with traces of other elements, aluminum (Al) containing alloys, and alloys without Al [25]. Typical Al-containing Mg alloys are AZ91, AZ31, AE21, calcium (Ca) modified AZ alloys and LAE442. AZ31 and

AZ91 have been used in technical applications for decades . There are many typical Al-free Mg alloy systems, such as WE, MZ, WZ, and Mg Ca alloys. The Mg alloy WE43 was developed to improve creep resistance and high temperature stability [68,71]. This alloy contains yttrium (Y), zirconium (Zr), and RE, respectively. Manganese-zinc (MZ) alloys have properties comparable to the ZM alloy system, a known system for forging applications in the transportation industry . However, almost none of the aforementioned alloys has been fully developed as a biodegradable implant material. Due to the complex alloy composition, it is uncertain whether the observed in vivo degradation is due to a chemical element, an intermetallic compound, or a microstructural effect based on the processing route [26].

2.3 CLASSIFICATION OF MAGNESIUM ALLOYS

For magnesium alloys, there exist a variety of different coding and identification methods, although none of them have yet reached widespread acceptance. For the purposes of this study, the terms for non-ferrous metal alloys defined by the American Society for Testing and Materials (ASTM) are employed. This nomenclature provides details about the alloy's composition and heat treatment. Each kind of magnesium alloy has its own name according to the American Society for Testing and Materials' (ASTM) classification system. This process may be broken down into four parts: the two most significant alloying elements are denoted by two letters in the classification's initial part. The most important alloying elements are listed in Table (2.2) [27] along with the letters that are used to designate them.

Table 2.1. Main alloying elements

A: Aluminum	B: Bismuth	C: Copper	D: Cadmium	E: Rare Earths
F: Iron	G: Magnesium	H: Thorium	K: Zirconium	L: Lithium
M: Manganese	N: Nickel	P: Lead	Q: Silver	R: Chromium
S: Silicon	T: Tin	W: Yttrium	Y: Antimony	Z: Zinc

The second portion of the categorization is made up of two numbers that represent the percentages of the two primary alloying elements. The third portion of the

categorization relates to a sequential letter issued by patent order, allowing distinguishing across alloys with the same alloy element content:

- A: First compositions, registered with ASTM
- B: Second compositions, registered with ASTM
- C: Third compositions, registered with ASTM
- D: High purity, registered with ASTM
- E: High corrosion resistance, registered with ASTM
- X: Experimental alloy, not registered with ASTM

Finally, the fourth part of this classification identifies the type of heat treatment or mechanic to which the alloy was subjected:

- F: As fabricated
- O: Annealed
- H: Strain hardened
- W: Solution heat treated
- H10 and H11: slightly hardened
- H23, H24, and H26: work-hardened and partially annealed
- T4: solubilization heat treatment
- T5: artificially aged
- T6: heat treatment of solubilization and artificially aged
- T8: solubilization heat treatment, cold worked, and artificially aged.

In general, magnesium alloys are classified into two types. The first category includes metal alloys that include between 2 and 10% aluminium and are mixed with other elements in lower average proportions, such as zinc and manganese. These alloys maintain suitable mechanical characteristics even when heated to temperatures as low as -120°C . The magnesium alloys that include components other than aluminium, such as rare earth elements, zinc, thorium, and silver, are the second category to be treated. Although these other elements are present, all of these magnesium alloys contain a trace amount of zirconium. This component is required because it enables the creation of a material with a smaller particle size, resulting in improved mechanical qualities. These alloys offer stronger mechanical characteristics at increased temperatures due to the use of more costly alloying components, and their manufacture

needs specialised methods. As a result, the price of this alloy has risen. Aside from the properties listed above, magnesium alloys have excellent machining properties, even at high cutting speeds. Furthermore, magnesium alloys can be welded in an inert gas environment, as shown in Table (2.3) for the most commonly used alloys containing a major alloying element such as aluminium (AZ, AM, AS, AE, and AT series). Another benefit of magnesium alloy over other metal alloys is that it has a lower melting temperature (between 650 and 680 °C, depending on the alloy) and takes less energy to melt . Magnesium alloys often compete with polymers in a variety of applications; nevertheless, it has a superior mechanical quality, greater resistance to ageing effects, improved electrical and thermal conductivity, and is simpler to recycle than plastic. However, due to a number of flaws, this material cannot be used on a large scale. The poor malleability of magnesium and its alloys at room temperature is the root cause of the material's most significant mechanical characteristics flaws. As a consequence, the number of skippable alloys available is restricted. As a result, casting or hot working at temperatures ranging from 200 to 350°C is the most efficient technique of creating components. Chemically, magnesium alloys are very brittle and prone to corrosion, particularly in marine conditions, and this is especially true of magnesium. When exposed to regular atmospheres, however, the wear resistance is adequate. When combined with weak creep resistance, these characteristics limit its use in a variety of applications with special requirements. Furthermore, there have been some concerns raised regarding the recycling of magnesium alloys. Even if the technical side of the equation is simplified, magnesium recovery circuits have yet to be integrated in manufacturing units. Finally, some economic issues must be considered, such as the fact that there are few manufacturers, which leads to an increase in the price of the final material [33].

Table 2.3. Common magnesium alloys and their applications [28].

Mg-alloy	Alloy Elements	Production	Properties
AZ91	9.0%Al 0.7%Zn 0.13%Mn	General casting alloy	Good molding, good mechanical properties at T <150°C
AM60	6.0%Al, 0.15%Mn	High pressure casting alloy	Higher toughness and ductility than AZ91, slightly lower strength. Often used in structural automotive applications
AM50	Mg-Al alloy	General casting alloy	Good strength, ductility, energy absorption and molding properties.
AE44	Mg-Al with rare earth system	General casting alloy	Better deformation and molding behavior than AE42
AE42	Mg4 atomic percentage Al2 atomic percentage rare earth	General casting alloy	Low molding level, good deformation behavior
AS41	4.2%Al, 1.0%Si	General casting alloy	Better creep resistance than AZ91 at high temperatures but lower strength
ZE41	4.2% Zn, 1.2% Terras Raras, 0.7% Zr	special casting alloy	The addition of rare earths improves the deformation resistance at elevated temperatures. Strong pressure.
AZ31	3.0% Al, 1.0Zn, 0.2% Mn	forged magnesium products	Good alloy for extrusion
AM20	Mg-Al alloy	casting alloy	High ductility, toughness, poor molding
MRI 153M	Mg-Al-Ca-Sr alloy	casting alloy	For high temperature applications up to 150°C
MRI 230D	Mg-Al-Ca-Sr alloy	casting alloy	For high temperature applications up to 190°C
AS 21	Mg-Al-Si alloy	casting alloy	For use at temperatures above 120°C
AJ62	Mg-Al-Sr alloy	High pressure casting	Good thermal and mechanical resistance, superior casting, corrosion resistance and deformation behavior

2.4 ALLOYING ELEMENTS

2.4.1. Aluminum (Al)

Aluminium (Al) is the third most abundant element found in the Earth's crust and is commonly found in its natural state in combination with oxygen and various minerals. Aluminium ranks third in terms of frequency among the elements. The material in question exhibits ductility at room temperature owing to its crystalline structure, which is face-centered cubic (FCC) in nature, thereby rendering it amenable to facile treatment. In contrast to other metals of a technical nature, aluminium exhibits a relatively diminished melting point of approximately 660 degrees Celsius. Aluminium exhibits a diverse range of capabilities, qualities, and physical, chemical, and mechanical characteristics, which manifest in numerous alloy variations. The fundamental characteristics of aluminium, including its significantly low specific weight, approximately one-third that of iron, may be briefly examined. This metal possesses favourable characteristics that render it highly amenable to various fabrication processes such as forming, rolling, drawing, extrusion, and welding, thereby making it an ideal construction material. The elastic modulus of the material in question is 70,000 MPa, which is three times less than that of iron, which is 200,000 MPa. Under loading conditions, the elastic elongation of the aluminium frame is three times greater than that of the iron frame. Aluminium and its alloys exhibit high resistance to various forms of corrosion. The metal's surface is perpetually covered with a layer of aluminium oxide owing to its strong chemical attraction to oxygen, which serves as an effective measure for averting potential corrosion. This characteristic renders them appealing in the domains of construction, naval engineering, and transportation, encompassing automobiles, locomotives, and aeroplanes. [29]. The previous studies have shown that the solubility in Mg is 2.6% wt. at room temperature and a maximum of 12.1% wt. at 436 °C. This decreasing solubility from the eutectic temperature gives the alloy the ability to heat treat and age. Mg₁₇Al₁₂ precipitate and solid melt Al are effective in improving mechanical properties. The most important disadvantage is that it increases microporosity. The Al content of many Mg-Al alloys is in the range of 2-9% and an optimum of 6% is recommended [30].

2.4.2. Tin (Sn)

Tin is a malleable metal that is silvery-white in color. Tin is corrosion resistant and does not oxidize easily due to the oxide coating that covers it. Seawater and municipal tap water cannot attack tin, but strong acids, bases, and acidic salts can cause damage. Because of its poor thermal conductivity, low density, and low elastic modulus, tin, whether pure or ethereal, is a valuable metal. moderate performance High reactivity with a range of other elements and strong corrosion resistance in a range of environments. Tin exists in two distinct forms or allotropes: the well-known beta or white tin and the less useful alpha or gray tin that is powdered. Reverse metamorphism, known as tin burn, occurs at low temperatures and severely limits the use of the metal in very cold locations [31]. Gray quickly turns white above 13.2 C, at temperatures above 100 C. The crystal structure of an atom is a tetrapod with its body at the centre. Both in its natural form and as a mineral, it has allotropic properties. It serves as a handle for materials that have a property known as the brittleness of the metal, and as a result its transformation is the same as the corrosion transformation. This is true because changing the metal is its primary function. High-resolution scanning electron microscopy (SEM) was used throughout the alteration process to allow researchers to assess the association between allotropes [32]. Figure 2.3 from earlier investigations illustrates the secondary phase of tin (Sn) with magnesium and its influence on the melting temperature.

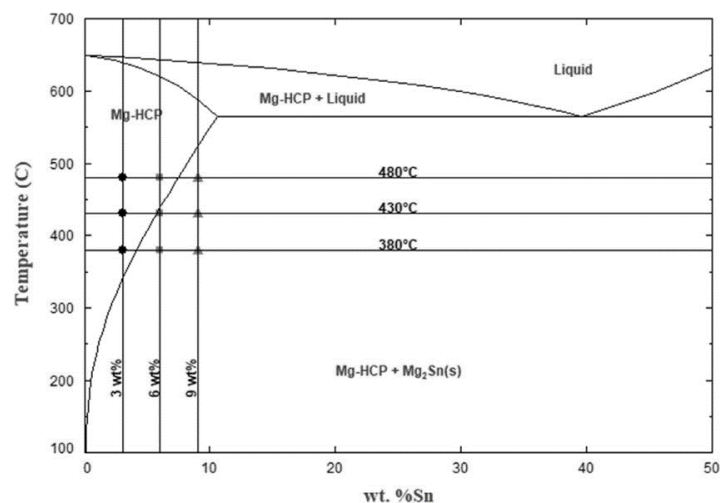


Figure 2.3. Mg-Sn secondary phase diagram [33].

2.4.3. Zinc (Zn)

Zinc ranks fourth behind iron, aluminum and copper in melting point (419.5 C) and boiling point (907 C). Its unbranched strength and hardness are better than tin and lead, but inferior to aluminum and copper. Pure metal is too brittle for demanding applications. For these reasons, zinc is commonly alloyed or plated with iron or steel. Zinc, unless extremely pure, is brittle at normal temperatures but becomes malleable at around 100°C and can be easily rolled, so plain wrought iron is typically used for full support zinc roofing. However, the addition of small amounts of copper and titanium increases the creep strength of coiled sheets, making them more useful for roofing . Compared to a demand of 13.77 million tons, the global zinc supply increased to 13.4 million tons [34]. Recycled zinc accounts for 2040% of global production [35]. 50% Zinc prevents corrosion from galvanizing steel. Zinc is biodegradable and can easily replace iron and magnesium [16]. Zinc-based alloys are made from 15% of the world's zinc. Forged ingots, drawn wire, applied extrusion and forged zinc alloys are offered. Latest zinc alloys for extrusion and forging are commercially available . Previous research showed the secondary phase of zinc with magnesium. As shown in Figure (2.4), MgZn₂ dissolves at 595 °C and becomes eutectic at 368 °C with a Zn concentration of 97%. This system lacks fixed melting regions [30].

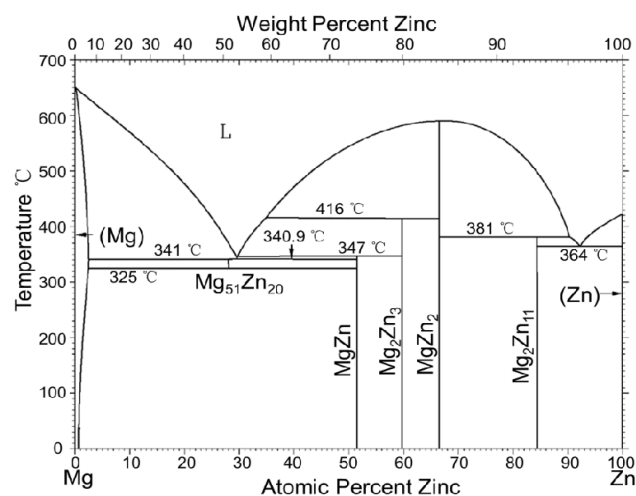


Figure 2.4. Mg-Zn secondary phase diagram [36].

2.4.4. Manganese (Mn)

Manganese (Mn) is a micronutrient needed by most organisms and chemically active in pink. It oxidises readily however is hard and brittle. Pure manganese interacts with air and water (rusting like iron) and dissolves in dilute acids. Manganese is needed to make steel and iron. 85% to 90% of overall demand is fulfilled by the steel industry. Manganese is utilised in numerous aluminium alloys and low-cost stainless steel compositions. Manganese also produces violet glass by decoloring glass . South Africa produces more than 82% of the world's manganese . Manganese steel is corrosion-resistant and inexpensive . Manganese's secondary phase with Magnesium was previously observed. Mn dissolves at 2% (atomic) at 653 °C. The Mg-Mn binary phase diagram (2.5) contains no intermediate composition [30].

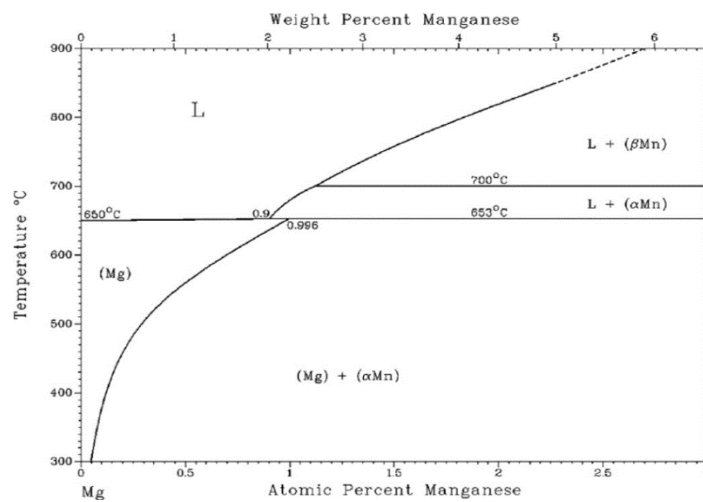


Figure 2.5. Mg-Mn secondary phase diagram [36].

2.4.5. Gadolinium (Gd)

Rare Mineral. Silvery, delicate, semi-elastic metal. Gadolinium forms a protective white oxide in moist air. It reacts slowly with colorless salts to form water and is extremely soluble in dilute acids. Compounds include trivalent elements. At 20 °C the magnetism of gadolinium is greater than that of nickel. At high temperatures, this metal forms binary nitrogen-sulphur-carbon-phosphorus-selenium-boron-silicon-arsenic compounds [37]. Most materials scientists use gadolinium to improve

numerous alloys. Rare earth elements such as Ce, La, Gd and Nd improve the corrosion and creep resistance of magnesium alloys. Rare earth metals create the intermetallic consolidation phase, which is stable even at high temperatures, and rare earth elements with high solubility form a solution in the -Mg matrix, a solid that yields magnesium and tough alloys. Deoxidation turns gadolinium silvery white. Gadolinium forms a black coating over time with oxygen or moisture. This temperature maximizes the magnetism of the element. Nature contains it only oxidized. Because of its chemical similarities, it usually contains rare earth impurities when separated [38]. Previous research showed the secondary phase of gadolinium with magnesium. Mg dissolves at the eutectic temperature up to 23.49% (in %Gd) as indicated in Figure (2.6), resulting in solid melt hardening [39].

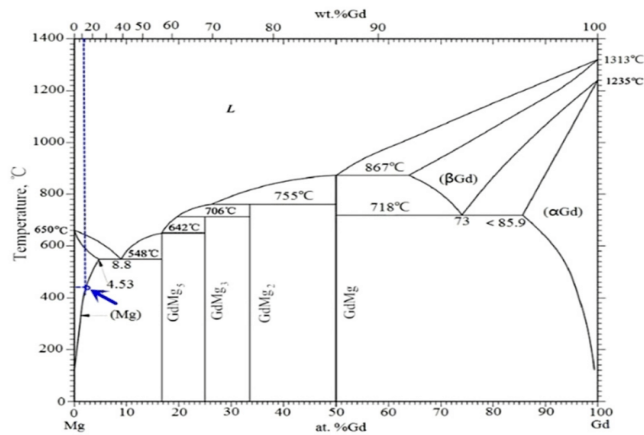


Figure 2.6. Mg-Gd secondary phase diagram [40].

2.4.6. Lanthanum (La)

Lanthanum is a soft, white metal that is easy to shape and shape. After europium, it is the most reactive rare earth metal. Lanthanum is oxidized to La₂O₃ in air at normal temperature. Although it interacts slowly with water, it quickly dissolves in dilute acids (except HF acid) due to the formation of a thin layer of fluoride (LaF₃) on its surface. Between 4 and 300 K (269 and 27) the magnetic sensitivity of the metal is almost independent of temperature, making it magnetic from 6 K (267 C) to its melting point at 1,191 K (918 C). Rare earth elements like lanthanum are often added to common alloys like magnesium and aluminum to increase their performance. These

improvements make the alloy more durable while reducing its weight, making it a very useful material in the manufacture of light but strong goods [38]. The yield point of magnesium alloys is improved by adding rare earth metals. The secondary phase of lanthanum with magnesium has been observed in previous studies. However, as can be seen in Figure (2.7), La has a very high eutectic temperature (612 C) and very poor solubility in Mg. Due to its limited resolution, it does not support the aging process [39].

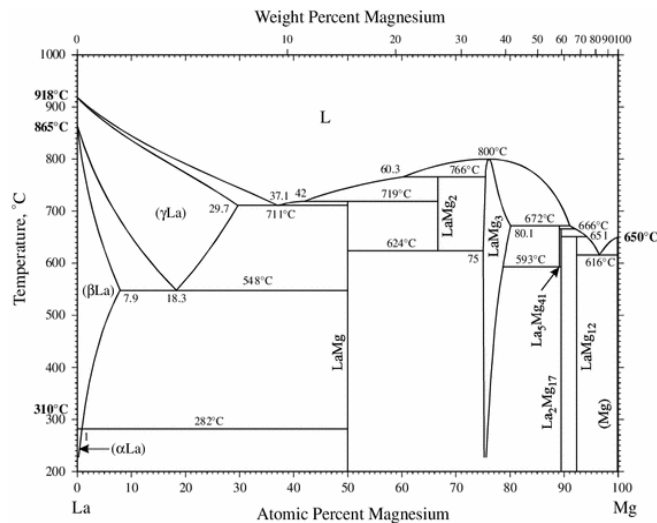


Figure 2.7. Mg-La secondary phase diagram [41].

2.5 AZ31 ALLOY

Aluminum is frequently used in alloying magnesium. Alloying can be done with a maximum resolution of 12.7% by mass, and AZ, AE, AM and AS series are obtained with the contribution of different elements. With Al additive, approximately 6% increase in strength can be achieved under optimum conditions compared to Pure Mg. The phase diagram of Mg-Al binary alloys is shown in figure 2.8.

Al-added Mg alloys are a frequently preferred material group, especially in orthopedics, due to their low densities and mechanical properties very close to bone tissue. AZ31 and AZ91 are the most preferred types in the Mg-Al binary system [42]. In addition to its mechanical properties close to bone, its corrosion resistance is quite high compared to pure Mg due to the presence of Al in the structure. With the

formation of Al_2O_3 during corrosion, a passive oxide layer is formed on the surface, thus increasing the oxidative resistance. This contributes to the biocompatibility performance. However, they are not suitable for long-term implantation due to the toxic effect of Al [43].

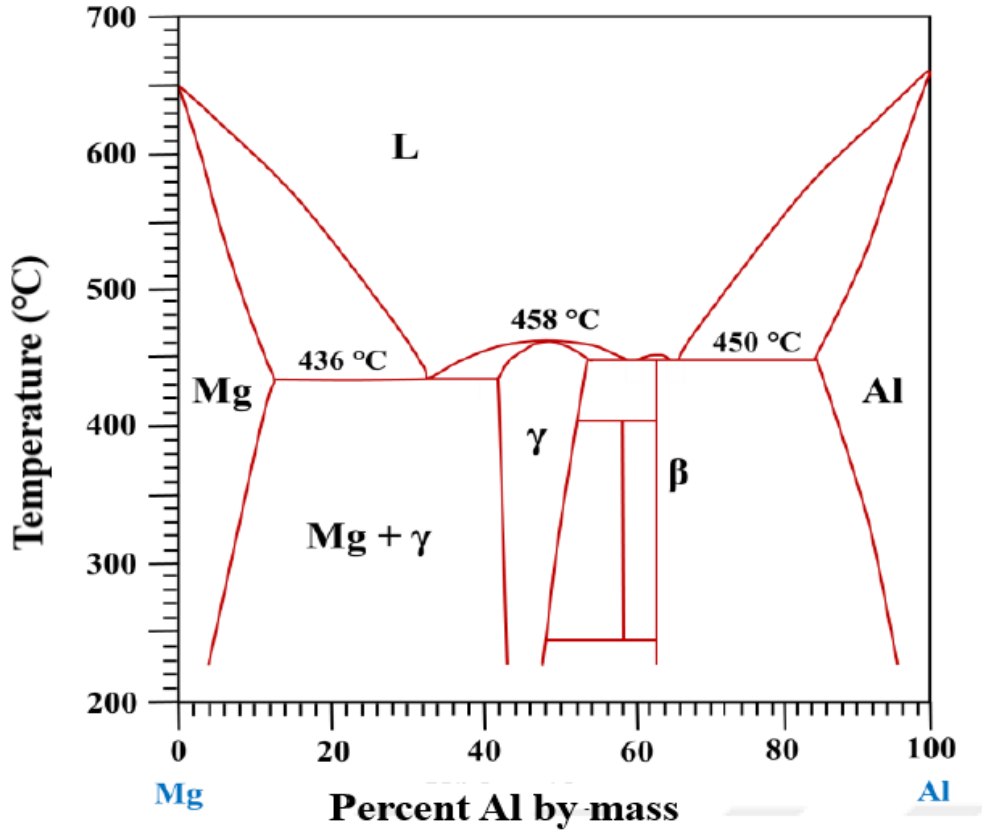


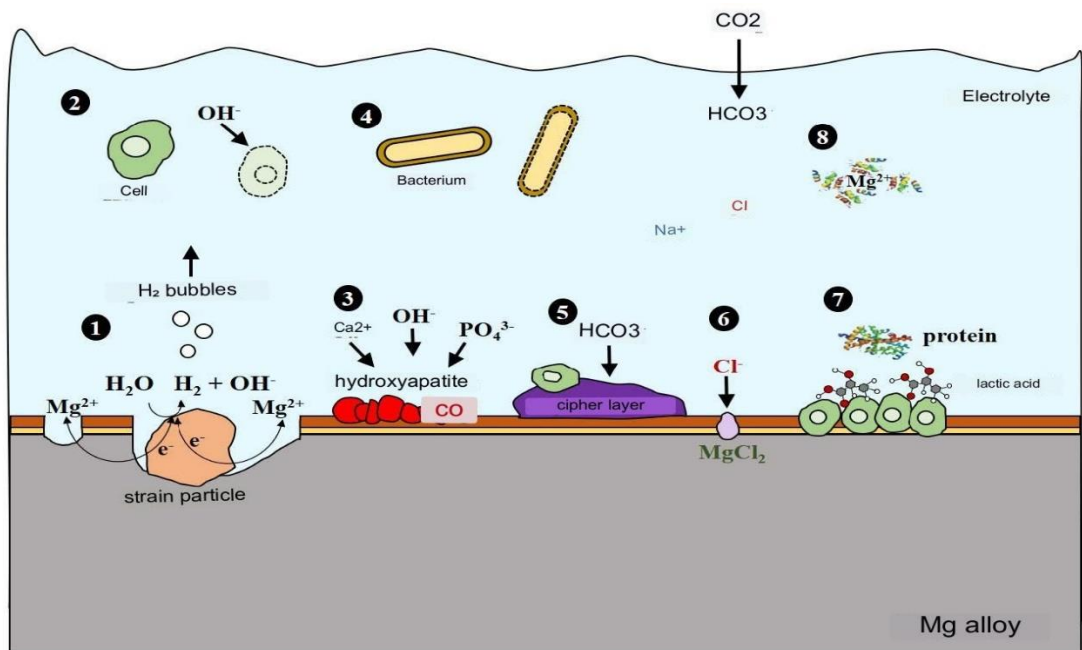
Figure 2.8. Mg-Al phase diagram[44].

2.6 BIODEGRADATION AND CONTROL OF Mg ALLOY

Changes in the physical and chemical properties of the biomaterial in a biological environment as a result of certain reactions and loss of material can be defined as biodegradability. In order for a biodegradable material not to adversely affect the healing time in the tissue it is in contact with, degradation is expected to occur gradually and over a period of time. In this context, magnesium and iron-based fully biodegradable alloys are required to interact with the effect of metabolic activities at an appropriate degradation rate [45]. Various advantages are obtained if biodegradable

metals are used for fracture fixation in the field of orthopedics (such as screws and pins). Mg and its alloys show a more successful performance in such applications due to the modulus of elasticity and mechanical properties close to the bone. In addition, Mg is a metabolite that should be consumed in the range of 250 - 300 mg daily and is stored in the bone naturally . Therefore, Mg alloys have an important place in the choice of temporary orthopedic implants. The spontaneous degradation process of a metallic material used for non-permanent orthopedic implants involves highly complex corrosion mechanisms. The same is true for magnesium alloys. Although Mg ions are not toxic, H₂ gas and alkalization that occurs during decomposition affect this process [46]. In addition, it is a significant disadvantage that most Mg alloys degrade in the biological environment with very high corrosion rates. Mechanical properties of Mg alloys weaken considerably during the three-month biodegradation period . Therefore, the use of biocompatible surface modifications as well as new alloys is an important alternative [6]. The method of the biodegradation mechanism of Mg alloys can be prepared by determining the material and surface character and in vitro environmental parameters. From this point of view, biodegradability studies are produced using different alloys, different surface treatments and different body fluids. Electrochemical measurements using these parameters provide information about reaction kinetics. The film formed by the corrosion products accumulating on the material surface is proven by the data obtained through these measurements. Different types of experimental approaches (such as corrosion, abrasion and tribocorrosion tests) allow for detailed investigation of biodegradation behavior. In addition, information about the concentration of metal cations can be obtained by solution analysis [6]. While performing in vitro experiments for biodegradation, the main goal is to provide the closest physical and chemical conditions to living metabolism. The test environment (solution) is an important parameter within the scope of this target. Body fluids, which play a vital role in the realization of metabolic activities, have a complex structure that contains many elements that are difficult to imitate. However, these complex structures are simulated with different kinds of artificial solutions that are constantly updated and have high simulation success. For a biomaterial with different degradation characteristics among a wide variety of solutions, the selection of the solution that best simulates the biodegradation mechanism improves the test quality. Magnesium and its alloys are very sensitive to aggressive solutions in terms of ion concentration. For this

reason, the test results obtained with buffer solutions containing different active substances provide a very strong interpretation of the corrosion mechanism for Mg and its alloys. The Cl⁻ ion in buffer systems containing HCl produces corrosive attacks on the magnesium surface [47]. Phosphate-based buffers change the chemical properties of the corrosion layer due to the phosphate ions they contain and form a precipitate on the surface [48]. More complex Mg²⁺ cations are seen in the use of protein-containing solutions. In Figure 2.9, the interactions that different biological environments can form in the Mg alloy are shown schematically [6].



1. Formation of Mg²⁺, H₂(g) and alkalization as a result of corrosion of 1 Mg.
2. The OH⁻ ion produced by the cathodic reaction related to Mg dissolution that damages the living cell.
3. The increase in pH triggers the formation of calcium phosphate on the alloy surface.
4. Bacteria die due to increased alkalization.
5. Carbonates form layers on the surface.
6. Chlorine ion attack occurs on the surface, MgCl₂ is formed.
7. Protein and cells adhere to the surface and produce lactic acid.
8. Proteins in solution complex Mg²⁺ cations.

Figure 2.9. Possible interactions between any Mg alloy and a biological environment [6].

The low density, specific strength and superior biocompatibility of magnesium and its alloys allow their widespread use as biomedical equipment [5]. However, low corrosion resistance and high degradation rate are the biggest disadvantages of these

alloys [8]. In particular, the dissolution rate of Mg and its alloys increases in the environment that is exposed to body fluids, and problems occur that affect the performance of the implant. After the implantation, excessive hydrogen release occurs and the healing rate in the bone tissue decreases. As a result of rapid degradation, local alkalization raises the pH value to its maximum value, which harms the living organism. With the release of Mg^{2+} ion, the osmotic pressure in the body fluid increases and the ionic concentration limit value is exceeded. In addition, mechanical damage develops as a result of decreases in strength due to structural defects during the use of Mg alloys for long-term treatment . These problems related to Mg and its alloys start as a result of the interface interaction between the material surface and the environment. Therefore, modifications made on the surface of a Mg-based biomaterial are effective in eliminating such problems.

2.7 BIOCOMPATIBILITY OF Mg ALLOY

Biocompatibility is a measure of how long a foreign material for the living organism will be accepted by the body [49]. It is a process that refers to post-biodegradation. In vivo, biological fluids have a corrosive effect on metallic materials. In this case, material loss begins, aseptic loosening and dangerous contamination of the surrounding tissues are observed. In this context, it can be said that the biocompatibility of metallic biomaterials is directly proportional to the corrosion resistance. The corrosion resistance of the metallic implant in the biological environment changes with some factors. Corrosion resistance can be improved with interventions, including in many surface engineering disciplines. In addition, if some noble elements (Au, Ag, Pt) are used in the implant material by alloying, the biocompatibility performance increases [50].

For implants selected from passive metals such as Co-Cr, Ti, Zr, Nb, Ta, the ability to form passive oxide film creates a barrier layer on the material surface and creates biocompatible implant performance. These oxides are sensitive to the previous electrochemical history of the surface. They change their structure and properties when exposed to different solutions and voltage conditions. In addition, the oxide film, which has been eroded as a result of the mechanical effect (tribocorrosion effect) together with the anodic potential, does not show equal corrosion resistance in all

regions . Although the corrosion resistance is quite weak, there are also elements with biocompatible properties and these species are in the group preferred as biodegradable. One of the most important of these elements is magnesium. Normal human metabolism contains about twenty-four grams of Mg. It takes part in vital metabolic activities such as protein synthesis, muscle and nerve activity, blood sugar control and blood pressure regulation . Compared to passive metals, it can be said that the biocompatibility degree of magnesium is very superior due to its natural structure of metabolism [51]. In addition, it has been determined that biodegradable magnesium implants contribute to the formation of a high amount of new bone in the region where it is bonded with bone [52]. The high concentration of magnesium ions released from the biodegradable implant ensures the activation of bone cells. In addition to all these advantages, some physical and chemical interactions that occur during biodegradation bring some disadvantages.

2.8. ELECTROCHEMICAL CORROSION

According to the ISO (International Organization for Standardization) 8044 standard, corrosion is defined as the physical-chemical interactions between the metal and its environment that cause significant changes in the surface properties and functional structure of the metallic material (ISO 8044 2020). These interactions often cause material losses. The formation and progression of the corrosion mechanism are directly related to the material type, the surface condition of this material and the environment. Considering these three parameters, it is necessary to study with interdisciplinary collaborations in order to fully explain the corrosion mechanism. It is possible to explain the types of corrosion that occur in different processes by using basic sciences such as physics, chemistry, biology, materials science [53]. The classification of the corrosion phenomenon is usually obtained by considering the formation mechanisms. The presence of a high chloride concentration is also considered to accelerate Corrosion of metallic implants, leading to metal ion release. Additionally, most metallic implants are undergone a static loading or a low-frequency cyclic loading. The corrosion damage of the metallic biomaterials is found in many forms like crevice, pitting, fretting, galvanic, wear, intergranular, and fatigue Corrosion. The attack rate

of general Corrosion is very low due to the spontaneous formation of passive surface layers on most metallic implants utilized at present .

2.8.1 Types of Corrosion

Depending on variables such as the type of metal involved, the type of corrosive environment, the geometry of the structure, etc., the presence of corrosion can manifest itself in a variety of ways. In most situations, the different forms of corrosive attack are classified based on the appearance of the alloy surface [54]. This section aims to provide an overview of the different types of corrosion failure processes, with a focus on those that most commonly affect magnesium and magnesium alloys. We therefore speak of the following types of corrosion

- i. Pitting Corrosion localized corrosion attack made on the resistant surface produces Pitting Corrosion. It commonly occurs on base metals protected by a naturally forming thin film of an oxide (for instance, the firmly adherent TiO_2 over the Ti surface) when the film's potential exceeds the oxide's breakdown potential in an aggressive environment. In the presence of given ions such as chlorides and sulfides, the film locally breaks down, and rapid dissolution of underlying metal occurs in the form of pits [55]. Figure (2.10) shows the pitting corrosion found on the magnesium alloy.
- ii.

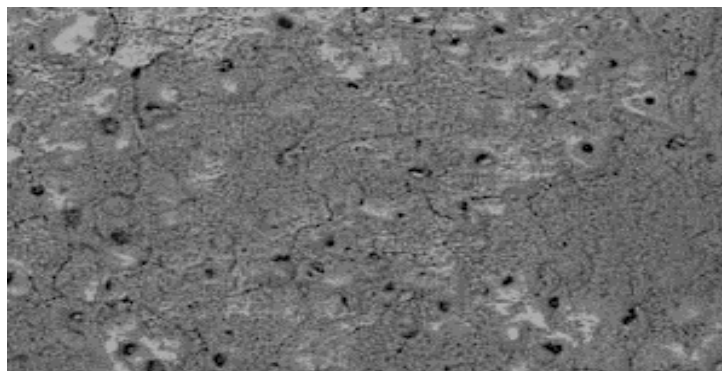


Figure 2.10. Pit corrosion of Mg alloys [56].

- iii. Intergranular Corrosion: this type of Corrosion happens because of technical errors and inhomogeneity, resulting in a more reactive nature of the grain

boundaries. The Corrosion of intergranular occurs adjacent to grain boundaries with comparatively very little Corrosion of grains [57]. Figure (2.11) shows intergranular corrosion on a magnesium alloy.

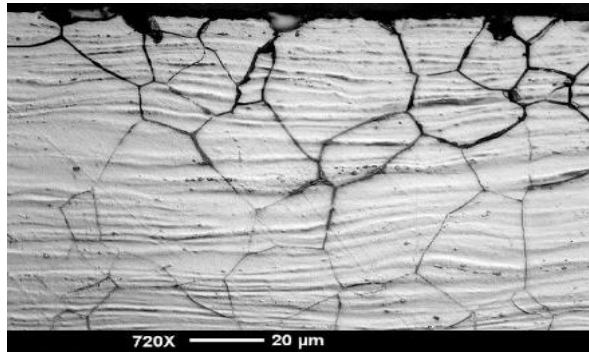


Figure 2.11. (IGC) of Mg alloys[56].

- iv. Fretting Corrosion is a form of erosion-corrosion and is considered the more critical form of Corrosion for implantology. Fretting Corrosion is a degradation process resulting from small movements' combined action between contacting parts and the environment's corrosivity. This can lead to tissue inflammation caused by the degradation of metallic materials used in prosthetic implants, leading to orthopaedic surgical operations [57].

- v. Galvanic Corrosion galvanic or two metal corrosion occurs when two different metals are in physical contact in an ionic conducting fluid media like a serum or interstitial fluid. In many practical applications, the contact of dissimilar materials is unavoidable. In surgical implants, galvanic Corrosion will occur if a bone plate and bone screw are made of different metals or alloys [58]. Figure (2.12) shows galvanic corrosion on Mg alloy.

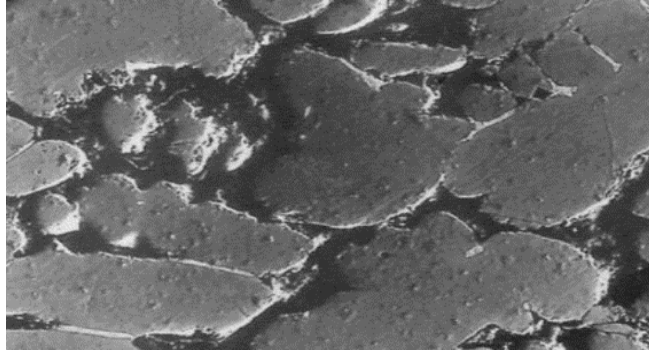


Figure 2.12. Galvanic corrosion of Mg alloys [56].

- vi. Crevice Corrosion occurs from the geometry of the implant/prostheses assembly. Corrosion of an alloy is more significant in the aperture's small sheltered volume created by contact with another material. The other metal could be part of the same or different alloy's fastener, a sheltered crown, cement packing, or implant prostheses joint [55].
- vii. Corrosion Fatigue is a fracture failure of metal due to the combined interaction of electrochemical reactions and cyclic loading. Corrosion fatigue resistance is an essential factor of consideration for load-bearing surgical implant metals or metals used in cyclic motion applications. Typically, a failure may not happen, but cracks can initiate from hidden imperfections, minute flaws, surface damage, chemical attack, and other causes [59].

2.8.2 Corrosion of Magnesium and Magnesium Alloys

Mechanism Equilibrium electrochemistry of an element in aqueous solution can be represented graphically using equilibrium cell potential and pH change. These graphs, introduced by Marcel Pourbaix and known as Pourbaix diagrams, are essentially phase diagrams in which the conditions for the thermodynamic stability of a single aqueous phase or its equilibrium with one or more solid phases can be determined. Pourbaix diagram of magnesium element in an aqueous solution is given in Figure 2.13.

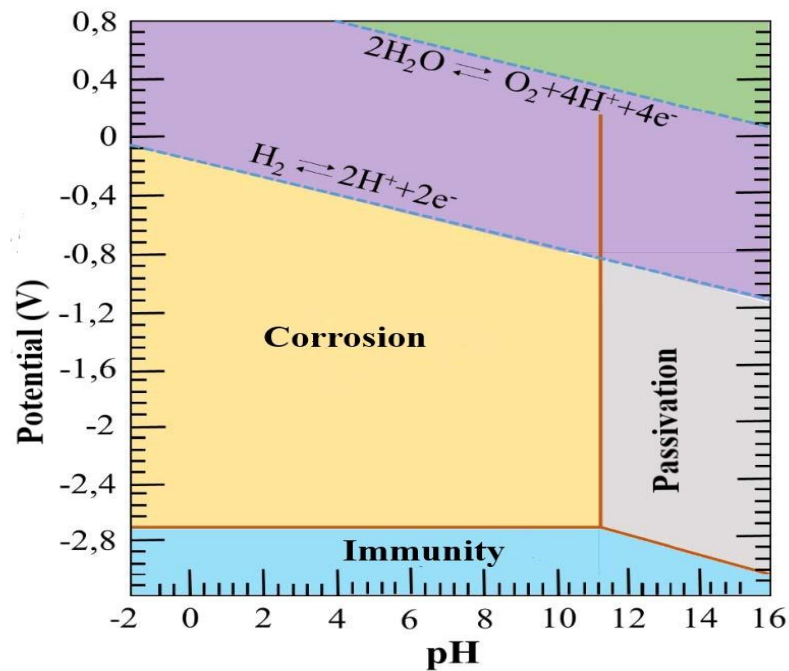
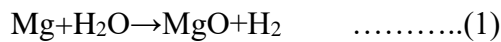
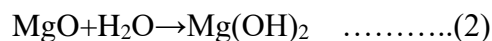


Figure 2.13 Pourbaix diagram of pure Mg element [57].

With the release of hydrogen in the immune region shown in Figure 2.13, the water molecule is reduced. Mg dissolves as Mg^{2+} . The passivation state in water occurs at the point where the pH value of the electrolyte is greater than 11.5. The oxidation of magnesium can be interpreted in two ways. The first state can be expressed by the oxidation reaction given in Equation 1. It is interpreted with the Pourbaix diagram with a thermodynamic approach.

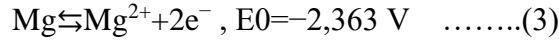


As the oxidation time is continued, the oxide film thickness on the magnesium surface increases. According to the Pourbaix diagram, $Mg(OH)_2$ formation takes place in the aqueous medium (Equation 2).

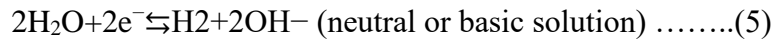
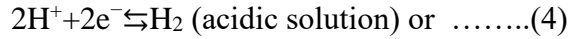


Hydroxide film has very low solubility in water. It is located in the outer shell on the sample surface. Corrosion resistance is weaker than magnesium oxide film [60]. These two films are formed not only during the corrosion of pure Mg element but also during

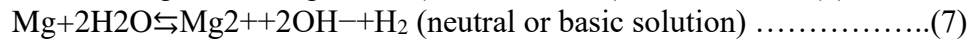
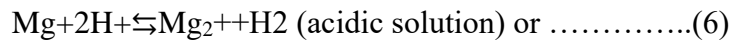
corrosion of Mg alloys [61] . In the second case, the effect of solution-dependent parameters is more dominant. Dissolution of divalent Mg is an anodic reaction;



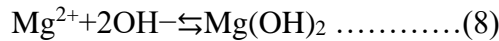
The anodic reaction is the simultaneous cathodic reaction,



It is possible. The total reaction can be written as shown in Equations 5 and 6:



The Mg^{2+} valence electrons reacts with the negative valence hydroxide ion, eventually forming metal hydroxide.



For Mg and its alloys, general corrosion occurs where there is poor electrolyte conductivity, where the large cathode versus the small anodic region is used. Local corrosion types are pitting, filiform and crevice corrosion. Corrosion attack on magnesium or magnesium alloy immersed in electrolyte usually takes place in an irregular form (Figure 2.14). Pitting corrosion deepens in certain areas where the anodic character is dominant on the sample surface. In solutions containing chlorine ions, attack usually results in pitting corrosion. In Mg-Al alloy systems, corrosion generally proceeds with the formation of pitting and continues as filiform [62] .

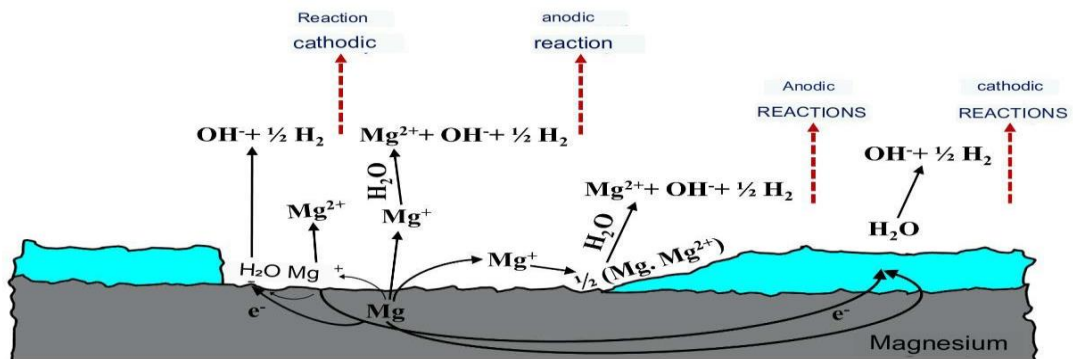


Figure 2.14. The anodic and cathodic reactions for the element magnesium [63].

2.8.3 Tribocorrosion of Mg Alloys

It is the damage that occurs as a result of effects that can change the mechanical and electrochemical properties of the surface at the same time. Such material damage can reach serious dimensions in terms of both safety and human health. Therefore, while the production processes are cascaded, measures should be taken to minimize the losses that may occur due to tribocorrosion. The analyzes required for these measures are performed by characterizing the synergistic and antagonistic mechanisms. There are four different approaches characterizing these mechanisms in the literature. In general, all parameters affecting the tribocorrosion mechanism are given in Figure 2.15 [64].

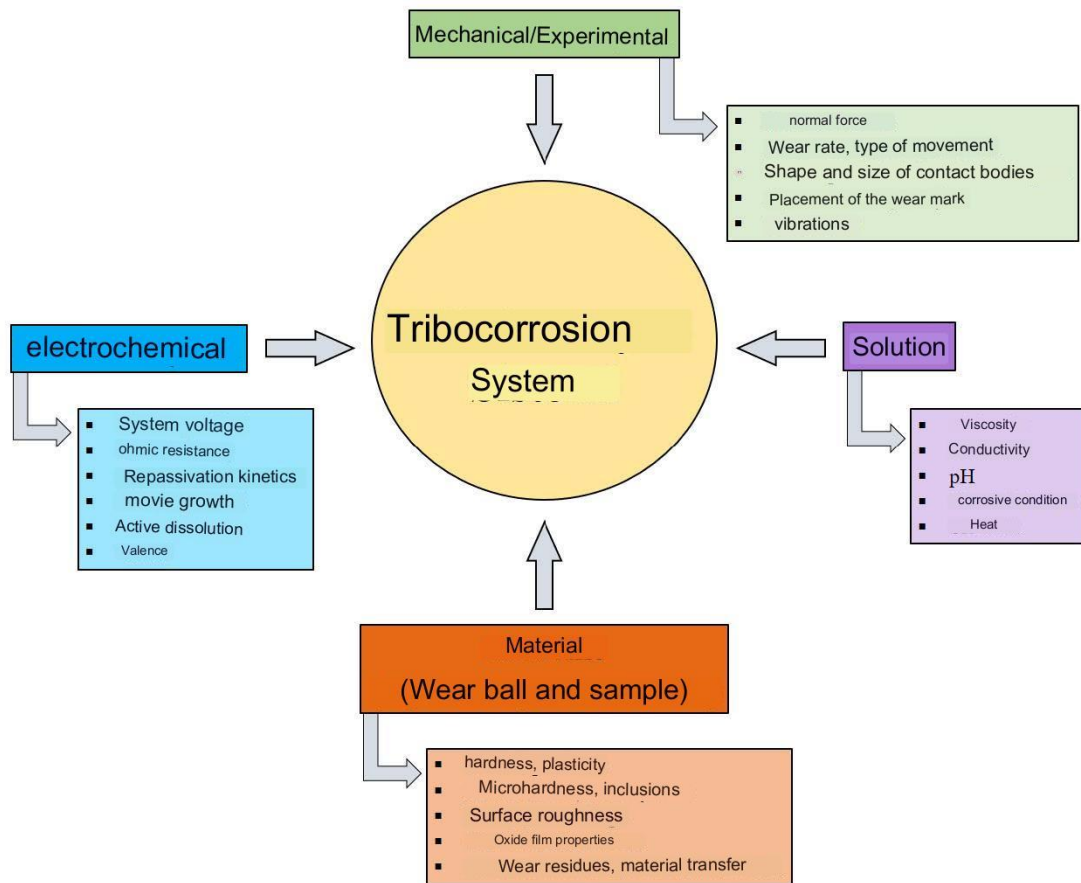


Figure 2.15 Four basic parameters affecting the tribocorrosion mechanism[64] .

Considering the parameters in Figure 2.15, many different methods have been developed for modeling the tribocorrosion mechanism. In order to understand the

intermediate stages in this mechanism, which works in a very complex order, electrochemical corrosion and wear-based experiments must be carried out and evaluated separately and cumulatively. This situation creates an intense need for measurement and analysis. Looking at the literature, it is seen that very different models are used for the analysis processes performed after the experiments [65]. Tribocorrosion is a dangerous process that can be seen in many different disciplines and causes significant material damage. For bioengineering, which is one of these disciplines, tribocorrosion is a mechanism that must be handled in a very complex order. The state of tribocorrosion within a biological system is called bio-tribocorrosion. The corrosive effect, accompanied by wear, is greatly affected by the ion concentration of the biological fluid. In addition, protein adsorption changes the electrochemical balance of the system and increases the rate of corrosion of the material used in the biomedical field in terms of bio-tribocorrosion [66].

The wear-corrosion balance for bio-tribocorrosion is analyzed as a synergistic effect with the modeling in the literature [67]. The synergistic effect approach was modeled by Watson et al. in 1995 [68]. According to this model, tribocorrosion is the result of the cumulative effect of wear and corrosion mechanisms. This effect triggers degradation processes that accelerate implant damage. The life of the implant is reduced. For this reason, degradation mechanisms that may occur with synergistic effect should be determined before implant design and material selection [66]. The synergistic effect of tribological effects and electrochemical reactions first begins with losses on the implant surface. Surfaces with appropriate wear rate and friction coefficient for metallic implants are obtained by applying ceramic coatings to the surface. However, this makes the bio-tribocorrosion process, which proceeds with an already complex mechanism, more complex. During tribocorrosion, the uneroded region of the material, whose surface morphology changes considerably with the coating process, exhibits cathodic character, while the eroded surface becomes anodic. Thus, new galvanic couples are formed on the surface. In addition, the presence of wear and corrosion products affects the process [64].

2.9 THE HEAT TREATMENT OF Mg AND IT'S ALLOY

Magnesium alloys are gaining popularity due to their many useful properties, including low density, high specific strength, strong dimensional stability, and recyclability. Magnesium alloys, the lightest structural metal, can be used in place of heavier metals such as steel and aluminum. Magnesium alloys have been increasingly studied and used in recent years. Industrial casting and semi-rigid forming have largely replaced plastic working in the manufacture of magnesium alloy products due to the limited ductility of the hexagonal packed structure (HCP). The formability of Mg and its alloys is limited because they deform at room temperature mainly by basal slip and twinning. Therefore, it is common to use high temperatures during the thermomechanical treatment. Whenever the temperature is above 300 C and the corresponding critical shear stresses are comparable, it is generally assumed that additional slip systems (prismatic and hierarchical) contribute significantly to the deformation. However, it has been hinted that twinning could remain strong even in hot environments. Researchers have focused on improving magnesium's plastic formability as the material grows in popularity in the transportation industry, where it can improve fuel efficiency by reducing vehicle weight. HSIANG and KUO tested the mechanical properties of magnesium alloys, AZ31 and AZ61, hot-extruded under ideal conditions. The constitutive relationship of the AZ31 alloy was established by Yu et al. published which showed a stress curve derived at different strain rates and temperatures. From NODA et al. it was shown that grain boundary slip dominates the stable deformation behavior of the AZ31 alloy [69] who studied the transition of the deformation mechanism under high-temperature uniaxial tensile deformation. However, nothing is known about how the microstructure of magnesium alloy AZ91 evolves. As part of the homogenization process, atoms spread across a concentration gradient. The core and the dendritic surface are both pathways for atomic diffusion. Temperature is the primary catalyst for atomic diffusion, which accelerates exponentially with increasing temperatures. The higher the temperature, the less time it takes for the mixture to become homogeneous. The time and temperature required for homogenization are alloy specific due to variations in atomic dispersion. Casting properties such as degree of separation and grain size are also influenced. Materials with high tin and bronze content (more than 8 percent Sn) are notorious for their extreme segregation. Diffusion

and homogenization of tin (phosphorus) bronze, silicon bronze and copper-nickel alloys are more time consuming and laborious than most other copper alloys. As a result, these alloys are often subjected to a rigorous homogenization process. Homogenization temperatures in these alloys are typically maintained at 50 C below the temperature of the solid, and soaking times range from 3 to 10 hours [59].

2.10 APPLICATION OF MAGNESIUM ALLOYS

The initial use of magnesium alloys is seen in military environments. At present, the use of low energy consumption and reduced gasoline emissions has spread to regions, particularly in the automotive industry, where such measures are imperative. The use of Mg alloys in the automotive sector can be traced back to the 1920s. The first use of the technology was seen in the engine pistons of the Indy 500 race car in the United States. It was reported that around 4 million tons of pistons were made in Germany in 1937. General Motors made an additional crankcase component for the 1931 Mg. In the 1970s, the automotive industry saw the emergence of transmission and air-cooled engine applications. The introduction of water-cooled engines as a solution to engine performance and overheating problems led to a decline in the use of Mg components, previously prevalent in air-cooled engines. Regardless of this fact, certain automotive components including the Mg seat frame, passenger door and steering frame have been manufactured by well-known brands such as Mercedes and BMW since the year 1990. In addition, as already mentioned, it is a suitable alloy for portable electronic devices in reference . The characteristic properties of magnesium alloy AZ31 make it a promising candidate for various applications. This material is widely used in automotive components such as engine blocks or hoods due to its favorable properties in terms of heat resistance and light weight, resulting in improved fuel efficiency. The aerospace industry uses titanium to make aircraft frames and wheels due to its exceptional resistance to corrosion compared to aluminum alloys. In addition, this substance is present in medical implants due to its biocompatibility and exceptional fracture toughness [56].

PART 3

METHODOLOGY AND EXPERIMENT

3.1 MATERIALS

In this study, AZ31 Mg alloy and modified AZ31 Mg alloys were studied as the main material. The raw rolls used for production are given in Table 3.1. Pure Mg, pure Al, pure Zn were obtained from Turkey, and master alloys were supplied from China. For the production, a custom-made low-pressure permanent mold casting method was used (Figure 3.1) and the casting conditions given in Table 3.2 were complied with. Pure Mg was first placed in the stainless steel crucible. When the temperature of 775 °C was reached, after 1 hour of waiting time, first pure Al and then master alloys were added to the crucible. Meanwhile, the molten metal in the crucible was stirred continuously. The final alloy addition was added to the pure Zn crucible and after 10 minutes of mixing, the molten metal was injected into the stainless steel metal molds with a temperature of 350 °C under 2-3 atm pressure.

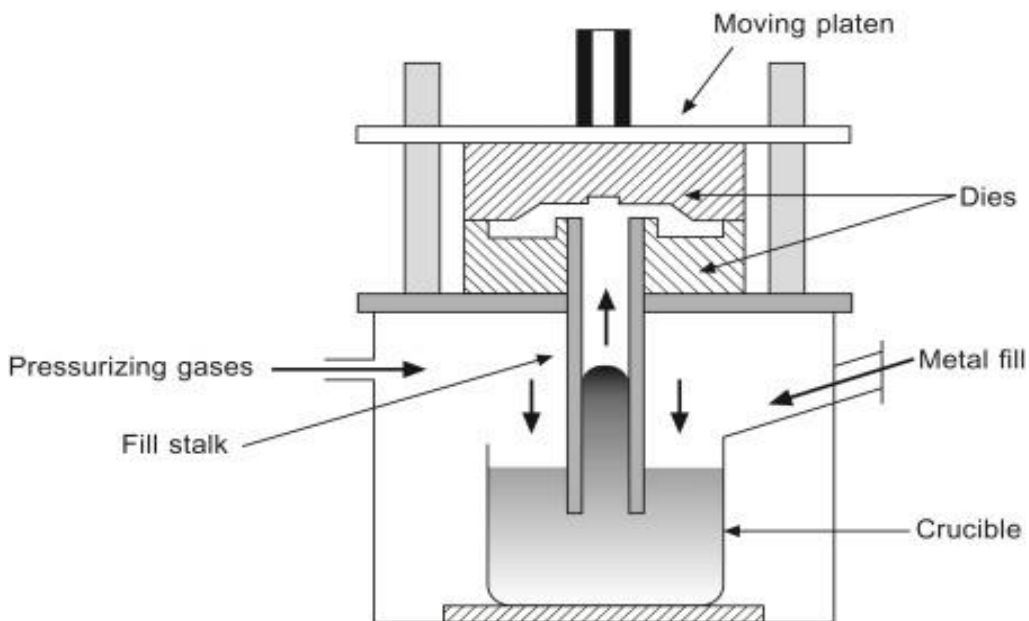


Figure 3.1 Low pressure permanent mold casting furnace [70].

Table 3.1. Casting conditions

Shielding gas	Melting Temp (°C) standby Time (minutes)	Mold Temperature (°C)	Runner Temperature (°C)	Casting gaz pressure (atm)
Argon	775-60	350	350	2-3

In this study the following alloys were used:

Z31, AZ31+0.5Nd+0.5La, AZ31+0.5Nd+0.25La and AZ31+0.5Nd+0.1La alloys were produced by induction melting method (Table 3.2) . figure 3.2 show experimental program of the present study.

Table 3.2 Alloying elements used in the study

Materials	Al	Mn	Zn	Nd	La	Mg
AZ31	3.62	0.11	1.18	-	-	Bal.
AZ31-0.5Nd-0.1 La	3.01	0.27	0.95	0.48	0.11	Bal.
AZ31-0.5Nd-0.2 La	2.92	0.15	0.91	0.49	0.23	Bal.
AZ31-0.5Nd-0.5La	2.88	0.25	0.87	0.45	0.54	Bal.

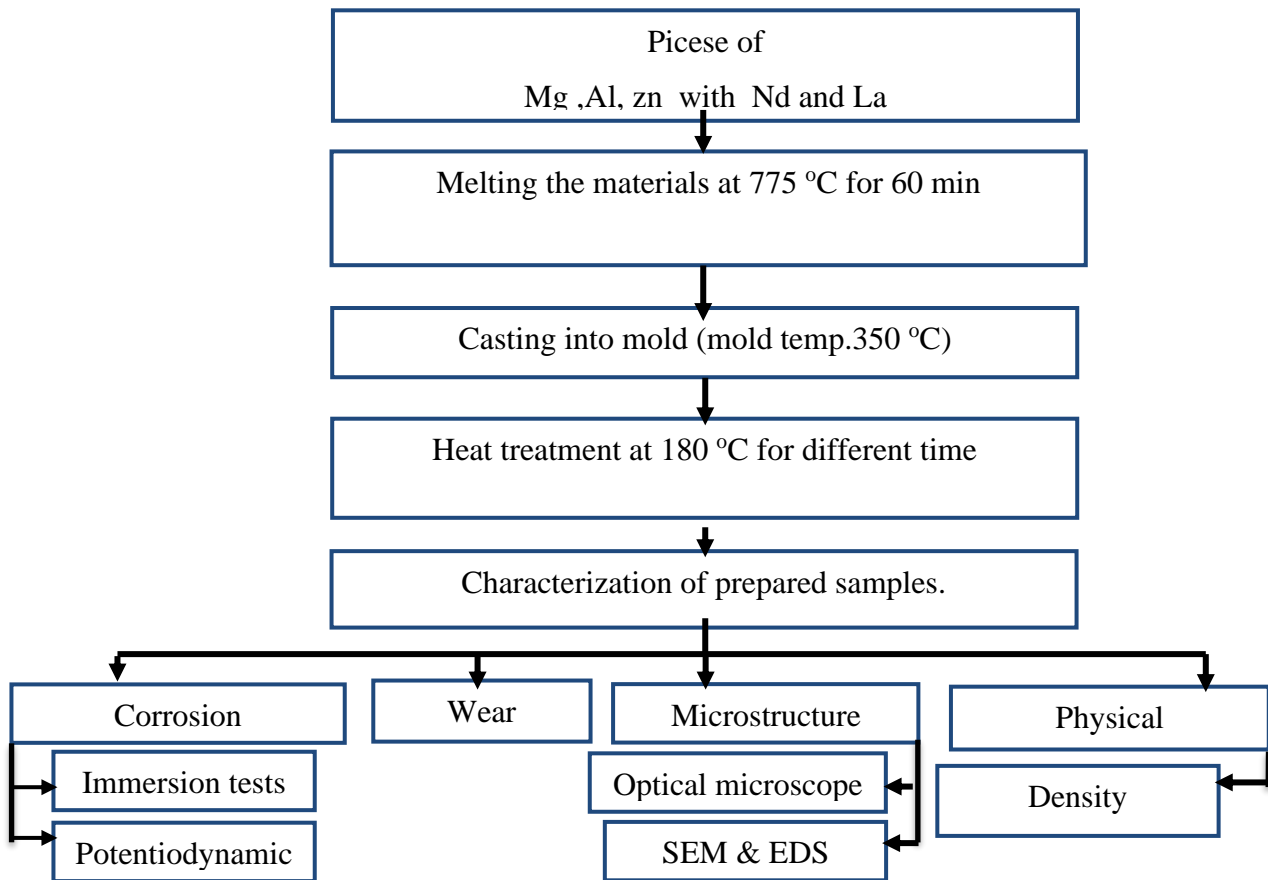


Figure 3.2. Experimental program of the present study.

3.2 PREPRATION OF SAMPLES TO TEST

3.2.1. Material Cutting

The materials were cut by the cutting device shown in Figure 3.3 according to different dimensions suitable for the type of tests used. Cut for corrosion tests to sizes of $1 \times 1 \times 0.5$ cm It was cut to a size of $2 \times 2 \times 1$ for the "wet and dry" wear test.



Figure 3.3. Cutting device used in the study.

3.2.2. Cold Bakelite

For ease of holding the samples and for carrying out corrosion tests, cold Bakelite was used, so that resin + color + hardener was used. The samples were poured into the mold and left for 24 hours, as shown in Figure 3.4. After the samples dried, they were taken out of the mold..



Figure 3.4. The cold bakelite mold used in the study.

3.3 HEAT TREATMENT

After the casting process, heat treatment was applied in order to eliminate defects such as segregation, inhomogeneous particle size and distribution that may occur in the cast parts. Heat treatment was carried out in the heat treatment oven shown in Figure 3.5 at a constant temperature "180°" and different times (10-20-30-40 minutes) and (1-2-3 hours). The samples were taken out of the oven and left to cool with air. Afterwards, the samples taken out of the furnace were cooled by immersion directly in water in order to preserve the homogenized structure. In this way, a more homogeneous microstructure and, accordingly, the same mechanical properties at every point of the cast part are provided.



Figure 3.5 Heat treatment furnace used in the study.

3.4 MICROSTRUCTURE CHARACTERIZATION

3.4.1. Microstructure

For metallographic examination in the optical microscope, the sample surfaces were sanded with 400, 600, 800, 1200 and 2000 mesh abrasives, respectively, using distilled

water. Then, the surfaces were polished using 1 μm alumina, and the surface was rinsed with distilled water and alcohol and dried. Picral's solution consists of (4.2 gr picric acid- 10 ml pure water- 70 ml ethyl alcohol – 10 ml acetic acid). Grains, grain boundaries, and secondary phases were examined in Conditions for size and shape distribution using A light microscope , as shown in figure 3.6.



Figure 3.6 OM device used in the study.

Then, SEM images and EDX analyzes were made with Carl Zeiss ultra plus gemini FESEM model scanning electron microscope in the Karabuk University Scientific Technology Application and Research Center (MARGEM) laboratory (Figure 3.7).



Figure 3.7 Carl Zeiss ultra plus gemini FESEM.

3.4.2. Physical Properties

The Archimedes principle performed density measurements in the sintered samples following ASTM B327, for which a Mitutoyo digital caliper with 0.001mm resolution and a Scaltec scale with 0.0001g resolution were used (Figure 3.8). The density of three samples from each group was calculated, and the average of these values was calculated according to equation 3.1.

$$p = \left[\frac{B-A}{(B-F)*D^o} * 100 \right] * D_W \dots \dots (3.1)$$

Where:

D_W – The density of water = 0.9956 g/cm³.

D^o - The density of oil= 0.634 g/cm³.



Figure 3.8. PRECISE XB 220A precision balance used in the experiments.

3.4.3. Immersion Corrosion Test

The experiments were carried out by constant immersion and electrochemical potentiodynamic polarization tests at 37 °C in two different solutions, the first being 3.5% NaCl and with SBF. For immersion and potentiodynamic polarization corrosion testing, the surfaces of the samples are sanded with sandpaper up to 1200 mesh.

Immersion corrosion tests were carried out in Immersion tests were carried out in a 3.5% NaCl solution for 4, 8, 16, 24 and 48 hours at a temperature of 37°C, samples of 8 mm diameter and 10 mm length were cut from cast alloys. The samples were sanded with 120 1200 SiC abrasive papers and cleaned with ethyl alcohol in an ultrasonic bath for 5 minutes before the test. Each sample was weighed (M_s) determined and surface area measured before starting the test, and then immersed in the corrosive medium for 4, 8, 16, 24 and 48 hours. Immersion tests were repeated three times. After each test, the corrosion products of the samples were removed by immersing them in an aqueous solution of chromic acid 182 g l⁻¹ for 5 minutes in an ultrasonic cleaner. Then it was washed with deionized water and placed in an ultrasonic bath in ethyl alcohol for 3 minutes. Finally, it was dried in warm air and then its mass was determined (M_f). The difference between the first measurement (M_s) and the last measurement (M_f) is determined as the corrosion mass loss.



Figure 3.9. Immersion test of AZ31 alloys.

3.4.4. Potentiodynamic Polarization Test

Since the extrusion process is carried out by taking the cylindrical ingot from the 35 mm part of the casting, the casting samples for the potentiodynamic polarization test were also taken from this part. Then, the prepared samples were wrapped with copper wire and covered with epoxy resin. The surfaces to be tested were sanded and cleaned with 1200 mesh abrasives. Then, an adhesive tape with a 0.25 cm² circular empty area at its midpoint was centered on the sample surface and adhered to, so that the corrosion tests of all samples were carried out in an equal area. In addition, the negative effects that may occur from the epoxy joints are eliminated in this way. Potentiodynamic polarization tests were performed at 37 °C in 3.5% NaCl and SBF with a computer-controlled DC105 corrosion analysis Gamry model PC4/300 mA potentiostat/galvanostat. Graphite rod was used as counter electrode, saturated calomel electrode (SCE) as reference electrode and classical three-electrode cell with sample surface as working electrode. Polarization curves were generated by scanning in the range of 0.25 V (vs. open circuit potential, E_{oc}) to +0.25 V (vs. E_{oc}) at a scanning rate of 1 mV.s⁻¹. Three potentiodynamic polarization tests were performed for each parameter and the average of the results was taken.

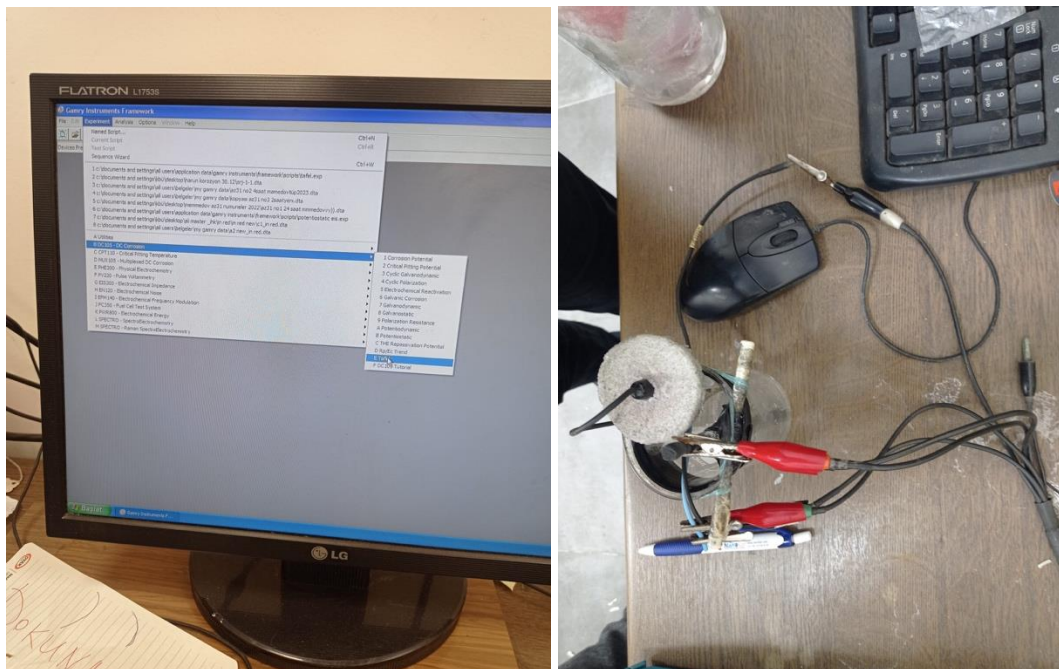


Figure 3.10. Potentiodynamic device used in the study

3.4.5 Wear Test

wear tests of casting samples were performed Wear tests are linear in UTS brand Wear tester according to ASTM G33 standard. It is performed dry and in synthetic body fluid (SBF) with back-and-forth motion type . Figure 3.11 A schematic representation of the wear test. It was measured under load (20 mm per cycle below 30 N) in SBD and without it consisting of Before the wear test, the samples were cut in accordance with the sample bed in the device, their surfaces were sanded with 1200 grit sandpaper and cleaned with distilled water and alcohol. The friction force during wear was measured by the load cell connected to the tribometer arm and instantly recorded in the computer. AISI 52100 quality high hardness steel ball is used as the insert material. Wear markarea, Mitutoyo brand SJ-410 model surface roughness device ISO 4287-1997measured according to the standard.

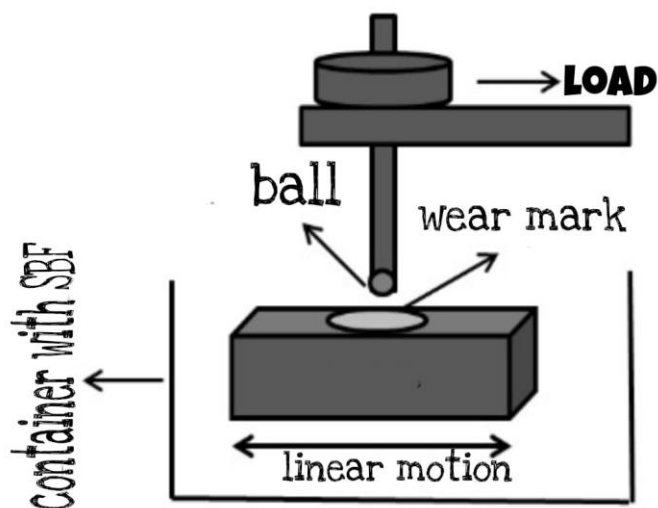


Figure 3.11. Schematic representation of the wear test [71].

PART 4

RESULTS AND DISCUSSION

4.1 INTRODUCTION

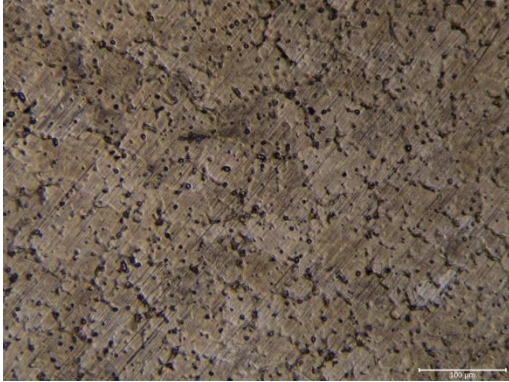
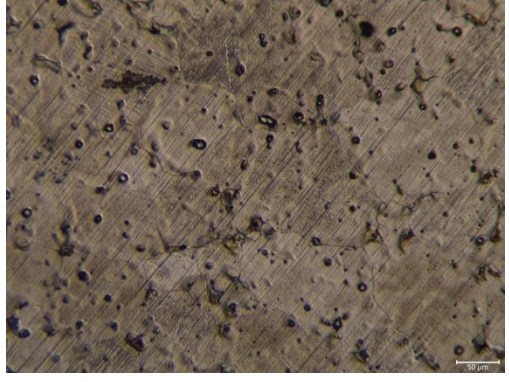
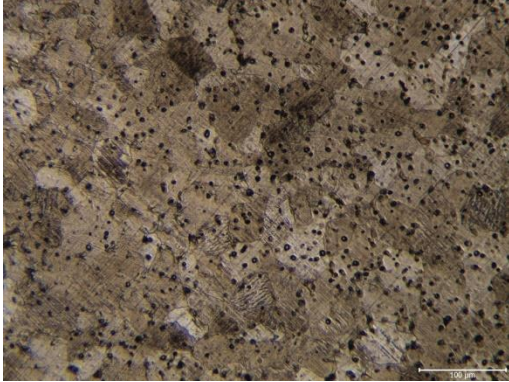
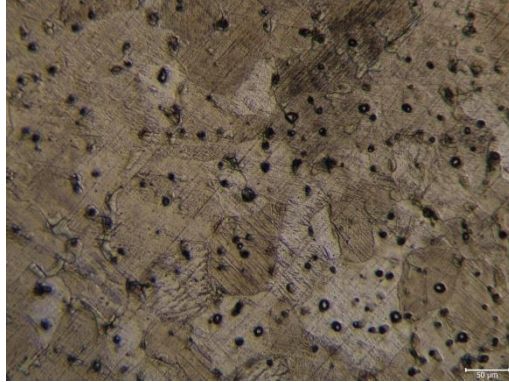
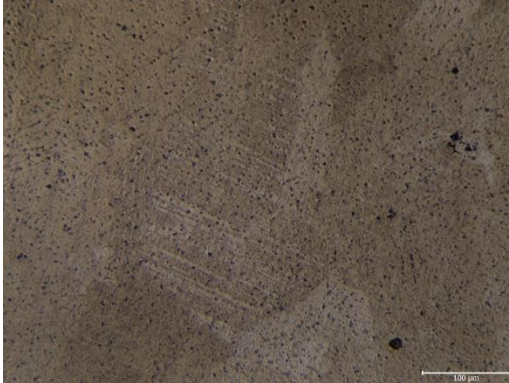

In this part, the characterization of prepared AZ31 alloys with and without different different concentrations of La and Nd element will be viewed by Optical microscope, SEM/EDS analysis. Wera test in dry and wet condition were analysis and electrochemical behavior of experimental specimens were also measured to show the suitability of these alloys for different applications.

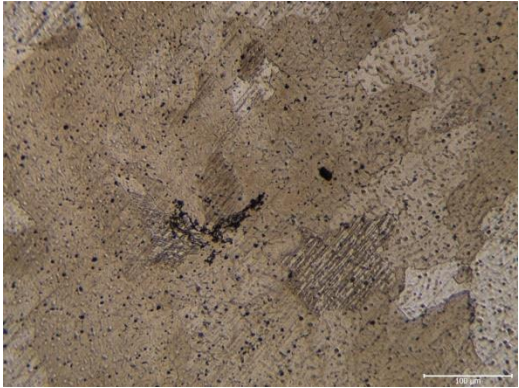
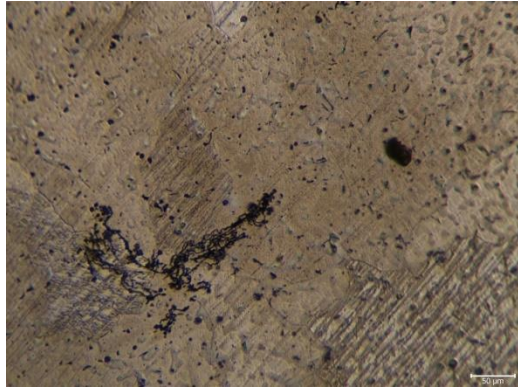
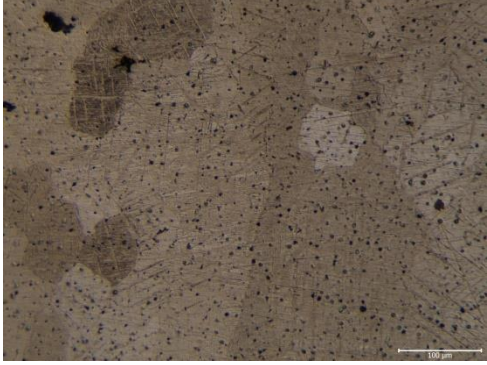
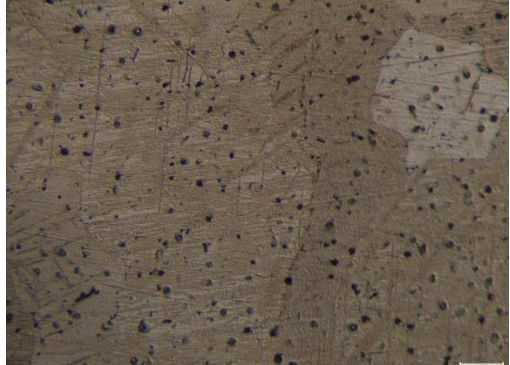
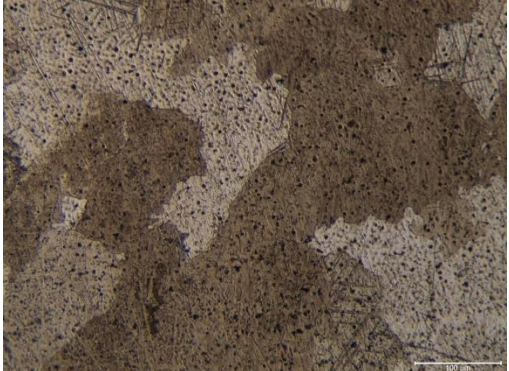
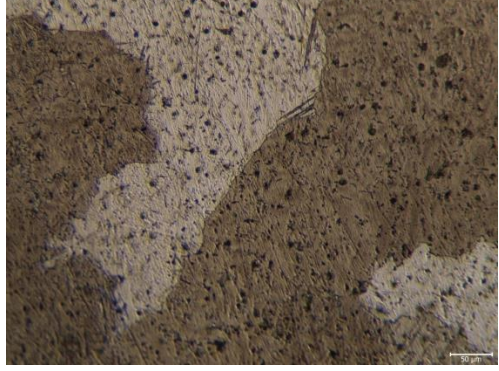
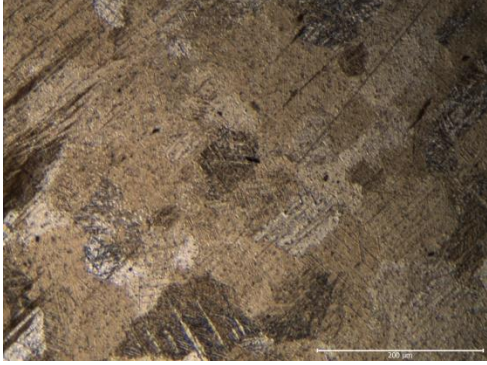

4.2. MICROSTRUCTURE CHARACTERIZATION

4.2.1. Optical Microstructure (OM) Analysis

In this study, the samples most and least exposed to corrosion were taken, and the microstructure was studied . In Table 4.1. are the optical micrographs of the heat-treated AZ31 samples. As seen in Table 4.1 . 0.2% La addition caused excessive coarsening in the grains of AZ31 Mg alloy. Despite this, it is seen that these coarsening grains become thinner with the addition of 0.5%La, but still maintain their size compared to the AZ31 Mg alloy. Grain boundaries are not clearly visible in the casting alloy with 1%La addition. In general, the addition of La decreased the clarity of the grain boundaries of the AZ31 Mg alloy and these invisible grain boundaries increased more due to the increasing La %.

Table 4.1 Optical micrographs of AZ31 .

	100 μm	50 μm
AZ31- 10min		
AZ31- 1 hour		
AZ31- 0.5Nd- 0.1 La -30 min		

<p>AZ31- 0.5Nd- 0.1 La - 1 hour</p>		
<p>AZ31- 0.5Nd- 0.2 La - 10 min</p>		
<p>AZ31- 0.5Nd- 0.2 La- 2hour</p>		
<p>AZ31- 0.5Nd- 0.4 L- 10 min</p>		

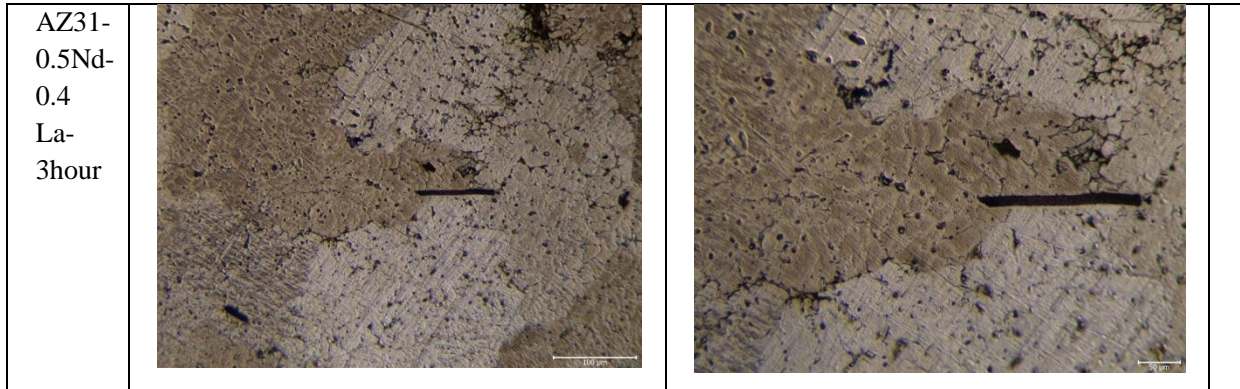


Table 4.1 Also it shows optical image images of AZ31 and Nd group Mg alloys. Here, Nd changed the structure of AZ31 Mg alloy, which contains homogeneous coaxial grains, to heterogeneous and different sized grains, while the fine and coarse grains were heterogeneous, the grains became more coarse with the addition of 0.5%Nd, however, with the addition of 1%Nd, there were still coarse and somewhat homogeneously dispersed equiaxed grains compared to the AZ31 Mg alloy.

Grain boundaries are more distinct after homogenization heat treatment. In addition, more homogeneous and equiaxed grains are observed compared to the casting microstructure. It is understood that the grains, which became excessively coarse after the addition of 0.2% La in casting, became thinner after homogenization . It can be stated that the AZ31 Mg alloys with La addition have similar grain sizes .

After homogenization, the 0.2% Nd addition alloy contains more homogeneous and equiaxed grains than the casting alloy . However, there was no significant improvement or change in the grains of 0.5%Nd and 1%Nd addition alloys . In addition, it can be said that the AZ31 Mg alloy contains finer grains than the casting .

Here, it was observed that the increasing La additions thinned the microstructure, and the grains became more fine with the increasing La addition. In addition, Al₂La and Al₁₁La₃ type secondary phases were discovered in the structure. It was observed that the secondary phases occupied more space by volume and mostly settled at the grain boundaries with increasing La addition. In addition, it has been reported that the Al₁₁La₃ phase has an acicular and lamellar morphology, and the Al₂La phase has a polygonal morphology [72]. Kumar et al. In their study, they produced Mg-3Al-xLa alloys and reported that the casting microstructure was thinned by about 50%, but different %La amount did not cause much difference in grain sizes. In addition, it has

been argued that La, which has a solubility of 0.78% (wt.) in Mg, produces more secondary phases by volume during cooling, thus leading to grain refinement. As a result of secondary phase analysis, rod-shaped $Al_{11}La_3$ and polygon-shaped Al_2La phases were found [73]. When the figure is examined, the cast state grains of AZ31 Mg alloys with 0.5%La addition first thinned, but increased in the addition of 0.7Gd, and then became extremely thin.

From the casting microstructure pictures of AZ31 and Nd group alloys, it was observed that the grains became coarser with increasing Nd and this was in agreement with the literature. Zhang et al. They reported that 0.38% (wt.) Nd addition of Nd added AZ31 Mg alloy made the grains coarser, however, 0.79% (wt.) Nd addition made the grains thinner, but it was still coarser than AZ31. In the case of electronegative difference, it has been said that the difference between Al-Nd is higher than the difference between Al-Mg and therefore Al is snatched by Nd. It has also been reported that Mg-Nd compounds are formed when Nd is increased.

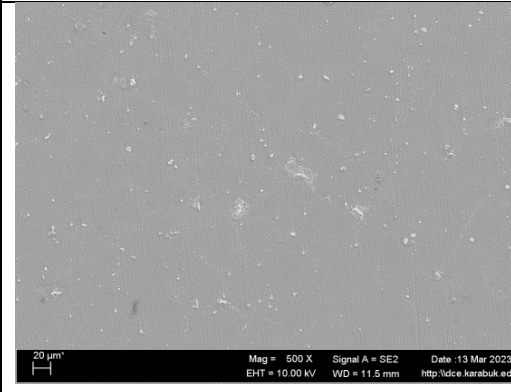
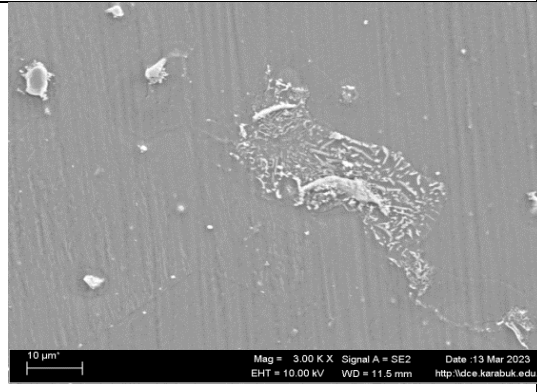
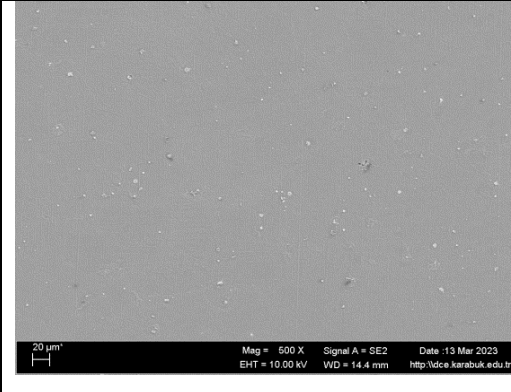
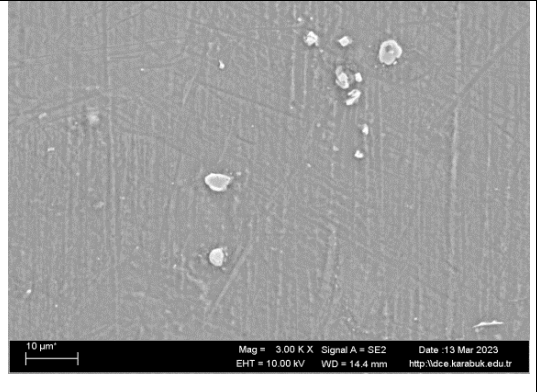

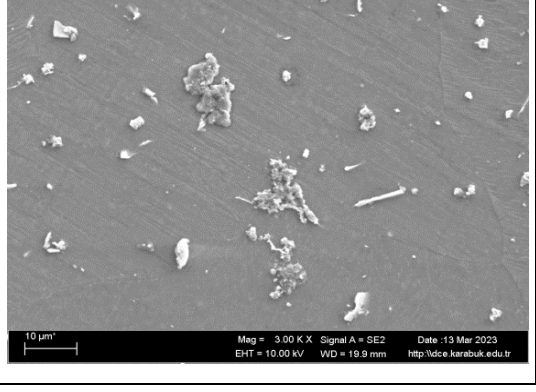
It is known that after homogenization, the unstable secondary phases dissolve in the structure [74] and the homogenization process improves the plastic deformation ability. After homogenization, equiaxed fine grains were formed in the AZ31 alloy containing 0.2% La, one of the La group alloys. Here, the La atoms diffuse slowly because they have a larger diameter, and thus the grains remain fine. However, since La solubility is very low in Mg, grain refinement is limited with increasing La amount [75]. However, the grains of the other alloys were partially coarsened due to the homogenization temperature.

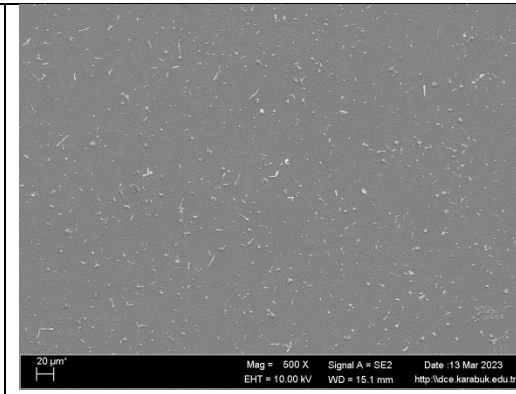
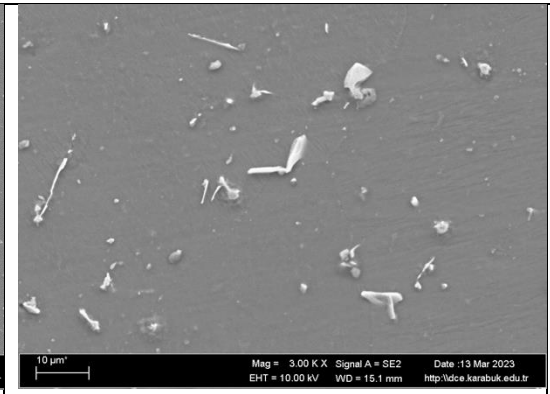
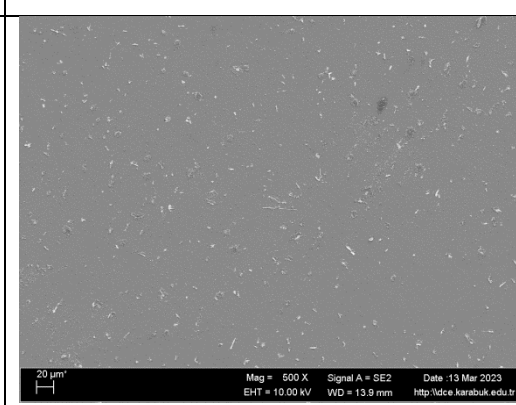

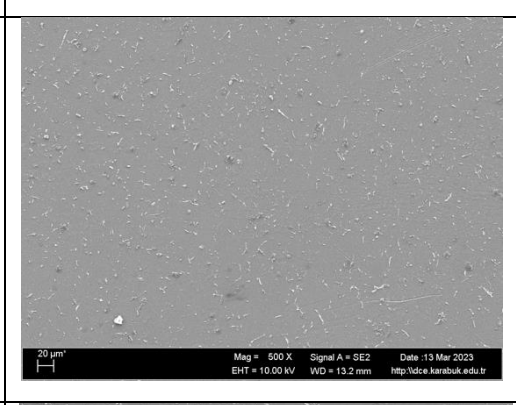
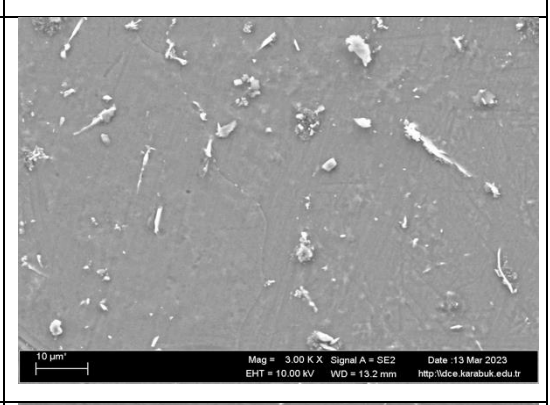
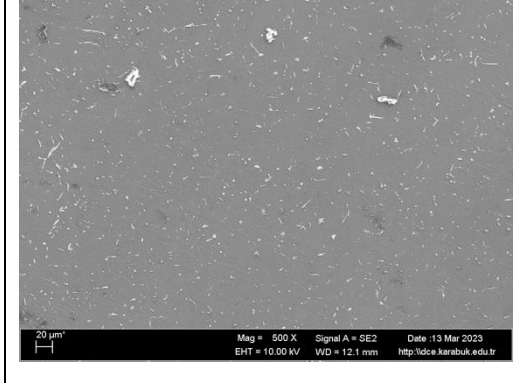
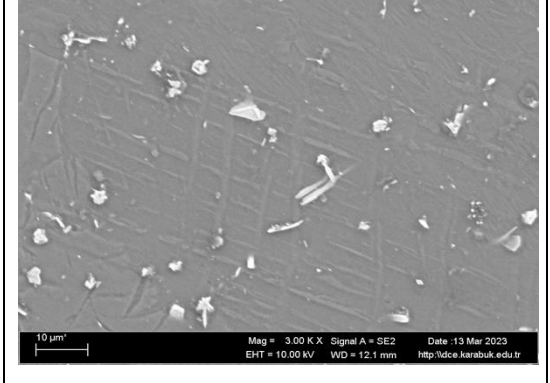
Optical Microstructure images of AZ31 alloy with the addition of La%-0.5 Nd, which has been subjected to heat treatments at a constant temperature (180°) and different times. It is noted from Table Table 5.2.1 that the crystalline borders are formed in most of the samples, and twinning is noted in some coarse grains in the alloys to which 0.5Nd and % La% are added. The grain size is large due to the slow cooling process after heat treatments.

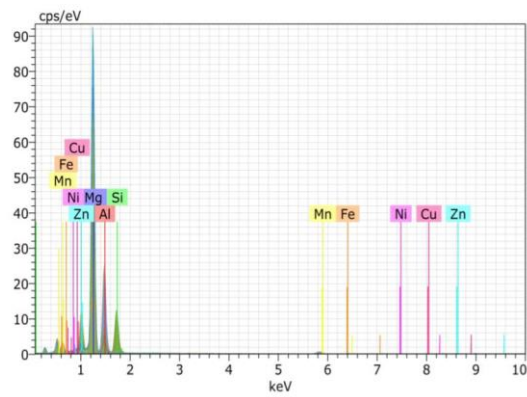
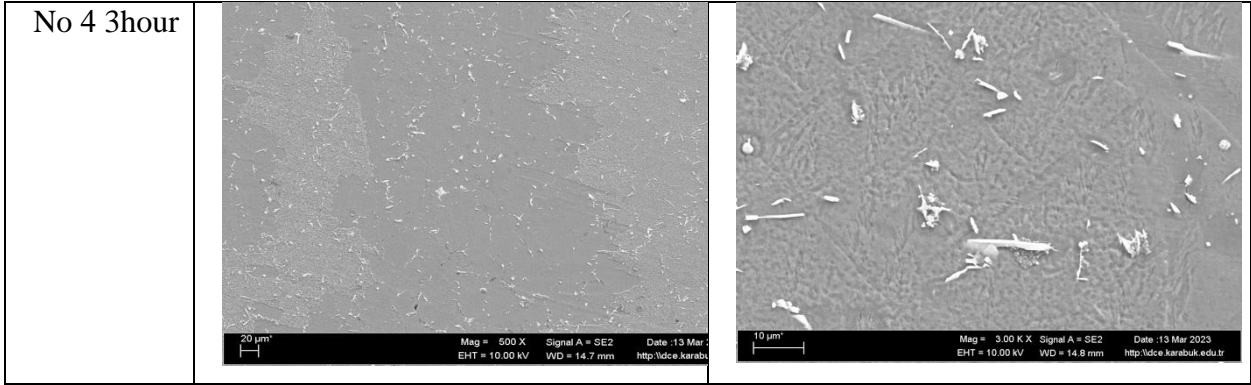
4.2.2. SEM analysis of Alloys

In Table 4.2. images of the SEM analysis of AZ31 samples. And in the figures (from Figure 4.1 to 4.8.) an EDX analysis of the samples.

Table 4.2. SEM and EDX of the prepared AZ31 alloy.

	500	3k
AZ31-10min		
AZ311 hour		
No 2 30 min		

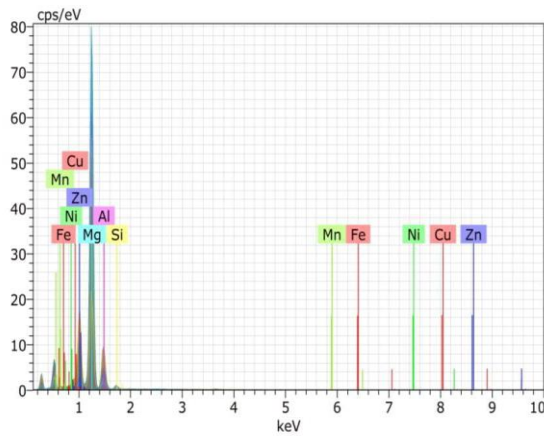
No 2 1 hour	 <p>20 µm² Mag = 500 X Signal A = SE2 Date :13 Mar 2023 EHT = 10.00 kV WD = 15.1 mm http://idce.karabuk.edu.tr</p>	 <p>10 µm² Mag = 3.00 K X Signal A = SE2 Date :13 Mar 2023 EHT = 10.00 kV WD = 15.1 mm http://idce.karabuk.edu.tr</p>
No 3 10 min	 <p>20 µm² Mag = 500 X Signal A = SE2 Date :13 Mar 2023 EHT = 10.00 kV WD = 13.9 mm http://idce.karabuk.edu.tr</p>	 <p>10 µm² Mag = 3.00 K X Signal A = SE2 Date :13 Mar 2023 EHT = 10.00 kV WD = 13.9 mm http://idce.karabuk.edu.tr</p>
No3 2hour	 <p>20 µm² Mag = 500 X Signal A = SE2 Date :13 Mar 2023 EHT = 10.00 kV WD = 13.2 mm http://idce.karabuk.edu.tr</p>	 <p>10 µm² Mag = 3.00 K X Signal A = SE2 Date :13 Mar 2023 EHT = 10.00 kV WD = 13.2 mm http://idce.karabuk.edu.tr</p>
No 4 20 min	 <p>20 µm² Mag = 500 X Signal A = SE2 Date :13 Mar 2023 EHT = 10.00 kV WD = 12.1 mm http://idce.karabuk.edu.tr</p>	 <p>10 µm² Mag = 3.00 K X Signal A = SE2 Date :13 Mar 2023 EHT = 10.00 kV WD = 12.1 mm http://idce.karabuk.edu.tr</p>



Mass percent (%)

Spectrum	Mg	Al	Si	Mn	Fe	Ni	Cu	Zn
1	94.28	1.64	0.02	0.37	0.08	0.57	0.81	2.23
2	52.34	9.14	22.13	0.41	0.00	0.54	1.94	13.49
3	18.22	37.16	1.65	14.00	2.87	0.70	3.60	21.81
4	22.19	35.26	1.20	9.07	1.64	0.21	3.51	26.93
5	83.00	9.48	0.09	0.00	0.05	0.54	1.32	5.53
6	88.53	6.40	0.08	0.00	0.00	0.58	0.72	3.70
7	87.58	6.38	0.44	0.78	1.13	0.07	0.46	3.17
Mean value:	63.73	15.06	3.66	3.52	0.82	0.46	1.77	10.98
Sigma:	32.70	14.68	8.17	5.66	1.11	0.23	1.31	9.98
Sigma mean:	12.36	5.55	3.09	2.14	0.42	0.09	0.50	3.77

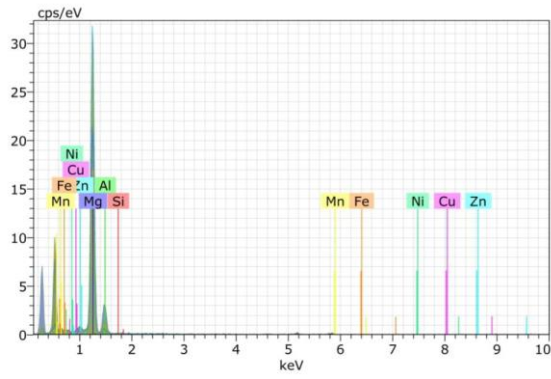
Figure 4.1 AZ3110 MIN



Mass percent (%)

Spectrum	Mg	Al	Si	Mn	Fe	Ni	Cu	Zn
1	92.26	3.03	0.14	0.00	0.00	0.53	0.74	3.31
2	52.04	18.38	0.24	0.58	0.04	0.46	3.55	24.71
3	84.71	6.31	2.98	0.00	1.04	0.27	0.74	3.97
4	35.93	15.07	0.09	0.40	0.00	0.40	6.68	41.43
5	83.42	9.23	0.16	0.00	0.00	0.35	1.11	5.73
6	80.47	10.94	0.16	0.00	0.40	0.22	1.04	6.77
Mean value:	71.47	10.49	0.63	0.16	0.25	0.37	2.31	14.32
Sigma:	22.23	5.62	1.15	0.26	0.42	0.12	2.39	15.51
Sigma mean:	9.08	2.30	0.47	0.11	0.17	0.05	0.98	6.33

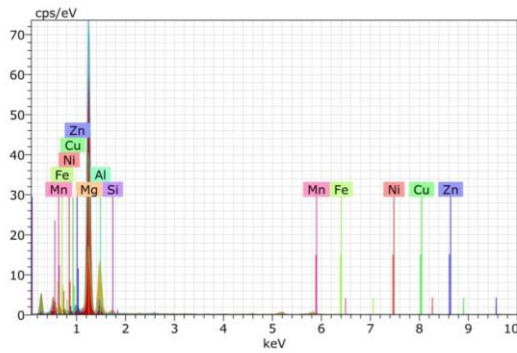
Figure 4.2 . AZ31 1 hour



Mass percent (%)

Spectrum	Mg	Al	Si	Mn	Fe	Ni	Cu	Zn
1	93.15	2.13	0.04	0.00	1.09	0.37	0.77	2.45
2	83.93	11.98	1.31	0.00	0.00	0.50	0.48	1.80
3	51.87	41.48	0.97	0.00	0.74	0.15	0.35	4.44
4	85.64	8.19	0.22	1.01	0.87	0.66	1.20	2.22
5	91.14	4.41	0.76	0.00	0.00	0.57	0.66	2.46
6	74.74	17.03	0.00	1.75	0.00	0.26	2.06	4.17
7	90.63	4.29	0.17	0.22	0.00	0.50	0.59	3.59
Mean value:	81.59	12.79	0.50	0.43	0.39	0.43	0.87	3.02
Sigma:	14.48	13.66	0.52	0.69	0.49	0.18	0.59	1.03
Sigma mean:	5.47	5.16	0.19	0.26	0.19	0.07	0.22	0.39

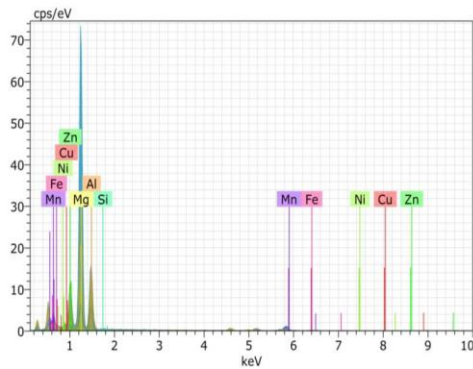
Figure 4.3. NO 2 30 min



Mass percent (%)

Spectrum	Mg	Al	Si	Mn	Fe	Ni	Cu	Zn
1	91.44	2.80	0.17	0.00	0.81	1.24	0.74	2.79
2	82.97	9.82	0.75	0.00	0.49	0.00	0.25	5.72
3	85.57	8.68	0.00	0.00	0.15	0.53	0.75	4.32
4	32.63	30.70	2.60	18.70	6.62	0.30	3.24	5.21
5	33.95	31.96	2.69	19.54	2.36	0.28	3.50	5.72
6	85.05	7.33	0.49	2.13	0.58	0.66	1.11	2.65
7	88.16	5.23	0.81	0.00	0.00	0.75	1.29	3.77
8	85.61	7.64	0.13	0.70	0.26	0.49	0.81	4.37
Mean value:	73.17	13.02	0.95	5.13	1.41	0.53	1.46	4.32
Sigma:	24.75	11.51	1.08	8.67	2.23	0.37	1.22	1.20
Sigma mean:	8.75	4.07	0.38	3.06	0.79	0.13	0.43	0.43

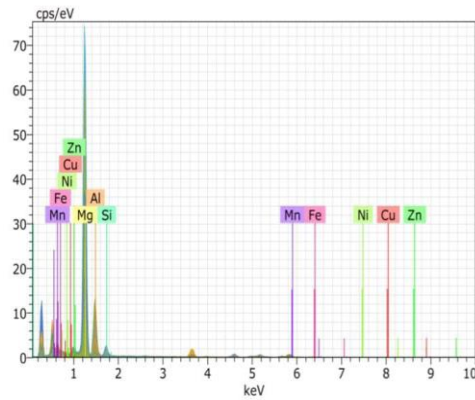
Figure 4.4. NO 2 1 hour



Mass percent (%)

Spectrum	Mg	Al	Si	Mn	Fe	Ni	Cu	Zn
1	92.11	2.60	0.22	0.61	0.00	0.65	0.55	3.28
2	45.90	24.74	0.07	0.20	0.19	1.04	2.69	25.17
3	43.58	24.85	0.18	5.68	0.82	0.57	3.21	21.11
4	40.18	31.34	0.23	15.29	3.83	1.31	1.81	6.00
5	13.15	34.63	0.36	34.44	8.66	0.64	3.50	4.62
6	67.09	22.67	0.00	2.76	1.78	0.25	0.39	5.06
7	34.06	49.94	0.00	2.45	0.49	1.96	1.39	9.71
Mean value:	48.01	27.25	0.15	8.78	2.25	0.92	1.93	10.71
Sigma:	25.18	14.30	0.13	12.43	3.12	0.57	1.24	8.80
Sigma mean:	9.52	5.40	0.05	4.70	1.18	0.22	0.47	3.33

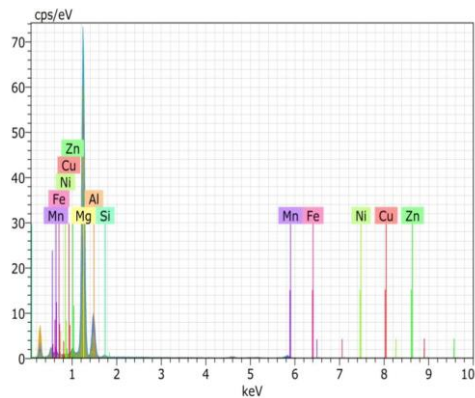
Figure 4.5 NO 3 10 min.



Mass percent (%)

Spectrum	Mg	Al	Si	Mn	Fe	Ni	Cu	Zn
1	93.55	1.84	0.08	0.00	0.43	0.51	0.80	2.79
2	25.49	30.96	0.53	24.35	7.97	1.66	3.82	5.23
3	40.89	25.48	11.71	3.13	3.88	2.57	3.25	9.08
4	64.21	28.22	3.99	0.00	0.23	0.00	0.22	3.14
5	89.43	4.37	0.66	0.14	0.00	1.10	0.56	3.72
6	45.98	23.91	8.35	4.93	3.23	2.59	3.71	7.30
7	90.66	4.73	0.22	0.00	0.74	0.50	0.64	2.51
Mean value:	64.32	17.07	3.65	4.65	2.35	1.28	1.86	4.83
Sigma:	27.60	12.78	4.66	8.90	2.91	1.03	1.64	2.52
Sigma mean:	10.43	4.83	1.76	3.37	1.10	0.39	0.62	0.95

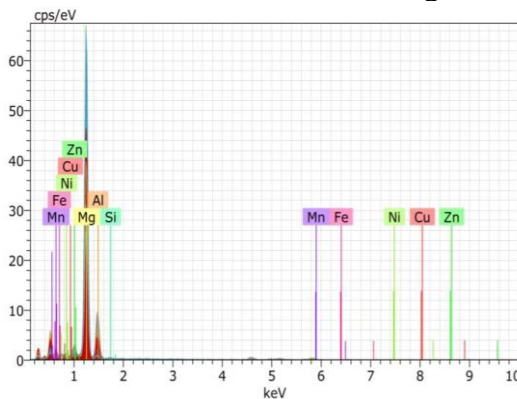
Figure 4.6 NO 3 2 hour



Mass percent (%)

Spectrum	Mg	Al	Si	Mn	Fe	Ni	Cu	Zn
1	93.45	2.04	0.00	0.00	0.48	0.33	1.09	2.62
2	85.81	6.98	1.15	0.71	0.44	0.62	1.21	3.08
3	74.09	19.72	0.89	0.00	0.03	0.28	0.42	4.57
4	90.22	4.93	0.62	0.09	0.25	0.12	0.72	3.05
5	47.95	23.72	1.14	17.38	4.54	0.62	1.47	3.18
6	83.35	8.01	0.40	0.00	0.00	1.20	1.58	5.48
7	66.93	24.67	0.00	0.63	2.35	0.32	0.00	5.10
Mean value:	77.40	12.87	0.60	2.69	1.16	0.50	0.93	3.87
Sigma:	15.90	9.51	0.49	6.49	1.70	0.36	0.57	1.15
Sigma mean:	6.01	3.59	0.18	2.45	0.64	0.14	0.22	0.43

Figure 4.7 NO 4 20 min



Mass percent (%)

Spectrum	Mg	Al	Si	Mn	Fe	Ni	Cu	Zn
1	95.22	1.70	0.12	0.00	0.03	0.44	0.43	2.07
2	94.13	2.55	0.20	0.00	0.00	0.47	0.58	2.07
3	54.40	28.63	0.65	2.14	1.43	1.82	2.46	8.47
4	70.07	17.27	1.09	0.00	0.00	0.71	1.66	9.19
5	89.91	5.01	0.00	0.36	0.00	0.47	0.57	3.68
6	94.14	1.82	0.09	0.29	0.12	0.42	0.80	2.33
7	56.33	19.84	0.01	14.30	4.15	1.71	0.74	2.92
8	80.70	13.03	0.06	1.53	0.90	0.35	0.40	3.04
Mean value:	79.36	11.23	0.28	2.33	0.83	0.80	0.95	4.22
Sigma:	17.07	10.07	0.39	4.90	1.44	0.61	0.73	2.90
Sigma mean:	6.04	3.56	0.14	1.73	0.51	0.21	0.26	1.03

Figure 4.8. NO 4 3 hour.

Table 4.2. shows the distribution of elements for AZ31 alloys, where the grains of aluminum, zinc and manganese appeared in a semi-circular form (manganese is semi-sponge-shaped) - and the elements added to AZ31 alloys (La and Nd) appeared in the

form of short threads. The figures (Figure 4.1 to 4.8) express the edx analysis where the constituent elements of each alloy were shown.

When the SEM images of AZ31 and La group alloys are examined after homogenization, it is understood that the grain boundaries of the AZ31 Mg alloy are more distinct. In addition, it is observed that the fine and large sized spherical secondary phases are formed in the grains and dispersed at wide intervals. However, AZ31 Mg alloy with 0.2% La addition contains homogeneously distributed secondary phases in acicular form and at frequent intervals. AZ31 Mg alloy with 0.5%La addition contains secondary phases formed in polygonal shape and generally at grain boundaries, as well as spherically formed within grains and grain boundaries. The AZ31 Mg alloy containing 1%La appears to contain more closely spaced thin spherical as well as thick rod-shaped secondary phases .

When the SEM images of the Nd group alloys are examined, it is seen that the secondary phases of the 0.2% Nd added AZ31 Mg alloy dissolve in the matrix after homogenization and contain a small number of thin spherical shaped secondary phases dispersed at wide intervals. AZ31 Mg alloy with 0.5%Nd addition contains homogeneously distributed coarse secondary phases at more frequent intervals. However, AZ31 Mg alloy with 1%Nd addition contains homogeneously distributed thin spherical secondary phases at frequent intervals .

4.3. THE PHYSICAL PROPERTIES RESULT

In Table 4.3. the density vakue for the prepared alloy . it can showd for the AZ31 without any addaition the density increase with increase the heattretment time and reached maxiumun when the time increased to 3 h. samples with addaition of La ithe result show that with increase the addaition concentration the density of the prepared alloy increased due to lowring the porosity and defect during the casting process and the due to increased the heat treatment time .

Table 4.3. Density for the prepared alloy .

alloy	Sample	Size (cm ³)	Weight(g)	Density (g/cm ³)
AZ31	AZ31-10min	0.1	0.17681	1.7681
	AZ31-20 min	0.1	0.17642	1.7642
	AZ31-30 min	0.1	0.17715	1.7715
	AZ31-40 min	0.1	0.17734	1.7734
	AZ31-1h	0.1	0.17728	1.7728
	AZ31-2h	0.1	0.17747	1.7747
	AZ31-3h	0.1	0.17748	1.7748
AZ31-0.5Nd-0.1 La	AZ31-0.5Nd-0.1 La -10 min	0.1	0.17749	1.7749
	AZ31-0.5Nd-0.1 La -20 min	0.1	0.17744	1.7744
	AZ31-0.5Nd-0.1 La -30 min	0.1	0.17737	1.7737
	AZ31-0.5Nd-0.1 La -40 min	0.1	0.17719	1.7719
	AZ31-0.5Nd-0.1 La -1h	0.1	0.17724	1.7724
	AZ31-0.5Nd-0.1 La -2h	0.1	0.17766	1.7766
	AZ31-0.5Nd-0.1 La -3h	0.1	0.17747	1.7747
AZ31-0.5Nd-0.2 La	AZ31-0.5Nd-0.2 La -10 min	0.1	0.17751	1.7751
	AZ31-0.5Nd-0.2 La -20 min	0.1	0.17721	1.7721
	AZ31-0.5Nd-0.2 La -30 min	0.1	0.17745	1.7745
	AZ31-0.5Nd-0.2 La -40 min	0.1	0.17762	1.7762
	AZ31-0.5Nd-0.2 La -1h	0.1	0.17742	1.7742

	AZ31-0.5Nd-0.2 L-2h a	0.1	0.17764	1.7764
	AZ31-0.5Nd-0.2 La -3h	0.1	0.17764	1.7764
AZ31-0.5Nd-0.5 La	AZ31-0.5Nd-0.5 La -10 min	0.1	0.17765	1.7765
	AZ31-0.5Nd-0.5 La -20 min	0.1	0.17745	1.7745
	AZ31-0.5Nd-0.5 La -30 min	0.1	0.17764	1.7764
	AZ31-0.5Nd-0.5 La -40 min	0.1	0.17732	1.7732
	AZ31-0.5Nd-0.5 La -1h	0.1	0.17747	1.7747
	AZ31-0.5Nd-0.5 La -2h	0.1	0.17753	1.7753
	AZ31-0.5Nd-0.5 La -3h	0.1	0.17757	1.7757

4.4. WEAR TEST

Figures (from 4.9 to 4.13) show induction diagrams for AZ31 samples under dry conditions and in a SBF .

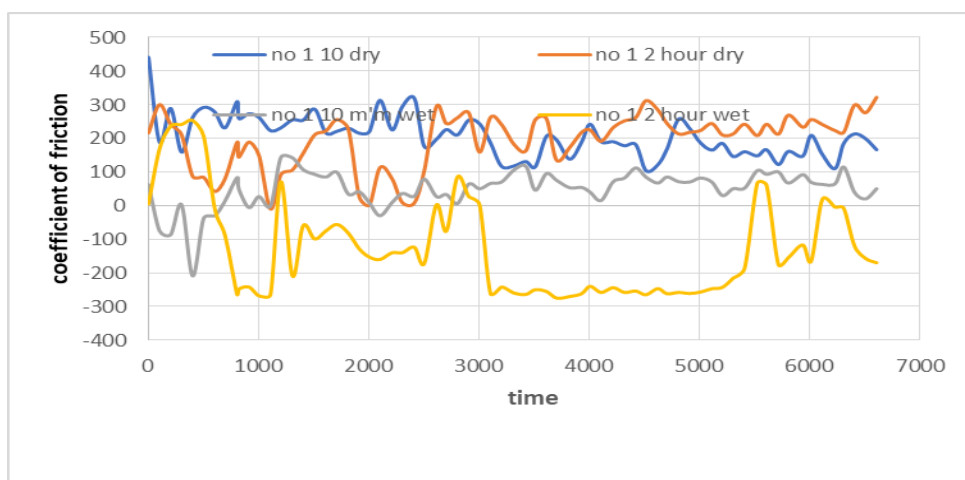


Figure 4.9. Wear diagram of AZ31

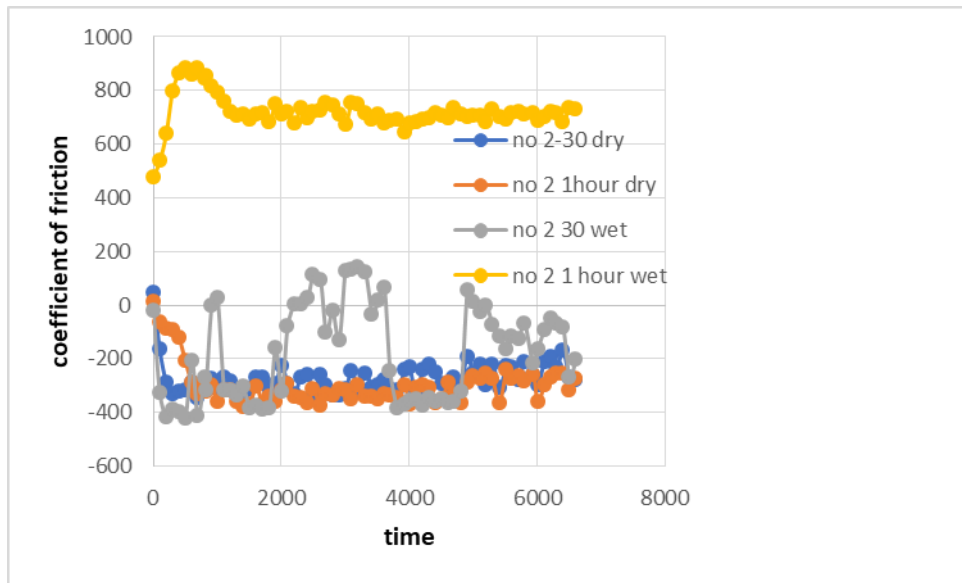


Figure 4.10. Wear diagram of AZ31-0.5Nd-0.1 La

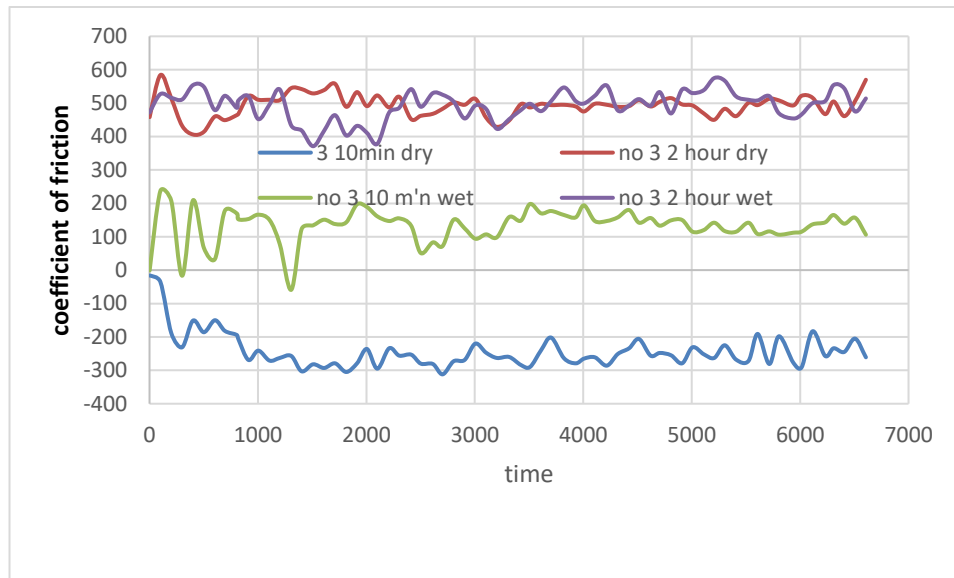


Figure 4.11. Wear diagram of AZ31-0.5Nd-0.2La

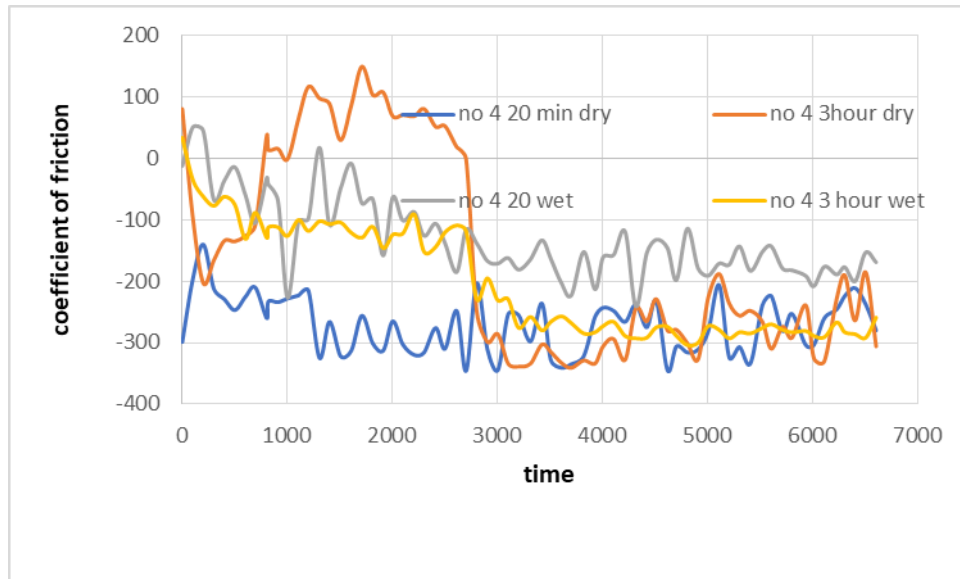


Figure 4.12. Wear diagram of AZ31-0.5Nd-0.4 La.

The figures (from Figures 4.9 to 4.12) show the wear diagram of AZ31 alloy. The experiment was carried out in a dry medium and a biological solution, where a load of 30 N was used for a period of 2 hours. It is noted from the figures that the rate of wear in the biological medium is greater than that of the dry medium, as the alloy AZ31-0.5 Nd-0.1 La-1h recorded the highest rate of wear in the bio-solution medium, and alloy AZ31-0.5Nd-0.2 La-2h recorded the highest rate of wear in the dry medium.

From the figure the weight losses, wear rates and average friction coefficients of casting and extrusion alloys obtained as a result of the wear test are given.

It is known that simulated body fluids have some effects on the wear behavior of Mg alloys. One and the most important is that it creates a beneficial lubricating effect to reduce the coefficient of friction. This can help prevent wear loss [76]. Another situation is that body fluids have a corrosive effect on Mg. Because the moment the Mg alloy comes into contact with the body fluid, an electrochemical reaction takes place immediately. This causes anodic and cathode reactions. After this interaction, different phases in the Mg alloy are thought to cause galvanic corrosion of the α Mg matrix. In addition, the protection film formed by corrosion is damaged by mechanical wear, which causes rapid corrosion and flaking wear debris also causes abrasive wear.

The wear effect of Hank's fluid makes the surface of the Mg alloy loose and porous, causing it to wear out more easily. At the same time, the Mg alloy is vulnerable to scratching under high load, causing the alloy to corrode easily. The two influencing factors act simultaneously on the Mg alloy and exacerbate the wear of the Mg alloy. In the literature [76, 77], the wear rate and the friction coefficient have generally given close results, since the amount of load applied in this study was 20 N and the distance was long, the current coefficient and wear rate different results were obtained. Possible intermetallics appearing in the microstructure after extrusion appear thinner and dispersed throughout the microstructure compared to the intermetallics in the casting microstructure. However, in the cast structure, these intermetallics appear more coarse-grained and extend along the grain boundaries.

4.5. ELECRTOCHEMICAL ANALYSIS

4.5.1. Immersion Corrosion Test Results

For the immersion corrosion test, the sample size is 10×10×10 mm. The area of each sample is calculated separately. weight measurements were made with Precisa brand precision scales. In the experiment carried out with the help of jars, each sample is placed in a jar in a net. immersed in a 3.5% NaCl solution and tested for corrosion tests 4, 8, 16, 8, 24 and Made within 48 hours. Corrosion on the sample surface at every hour interval . in the immersion test, it was observed from Figure 5.13 that AZ31-10 min has the most weight loss and that AZ31-0.5Nd-0.5 La- 3 hour has the least weight loss. It is also noted after 24-48 hours from the beginning of the immersion, the amount of weight loss is less than the previous readings due to the formation of a salt substance and the dissolved elements in the immersion solution on the surfaces of the studied samples.

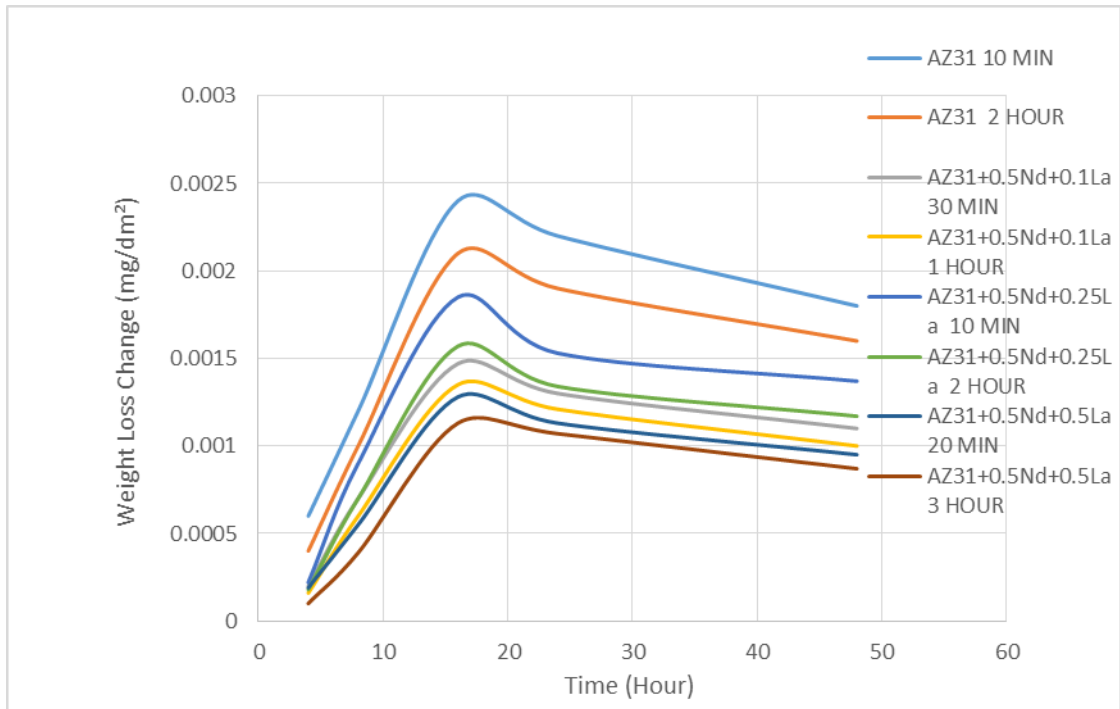


Figure 4.13. Corrosion immersion test diagram for AZ31 samples.

4.5.2. Potentiodynamic Polarization Corrosion Test Results

Corrosion experiment was carried out on two solutions, one of which is 3.5% NaCl saline, and the other is bio solution

Figures (from Fig 4.14 to 4.17) shows corrosion diagrams in brine , Table 4.4 shows the I_{corr} and E_{corr} values for AZ31 samples.

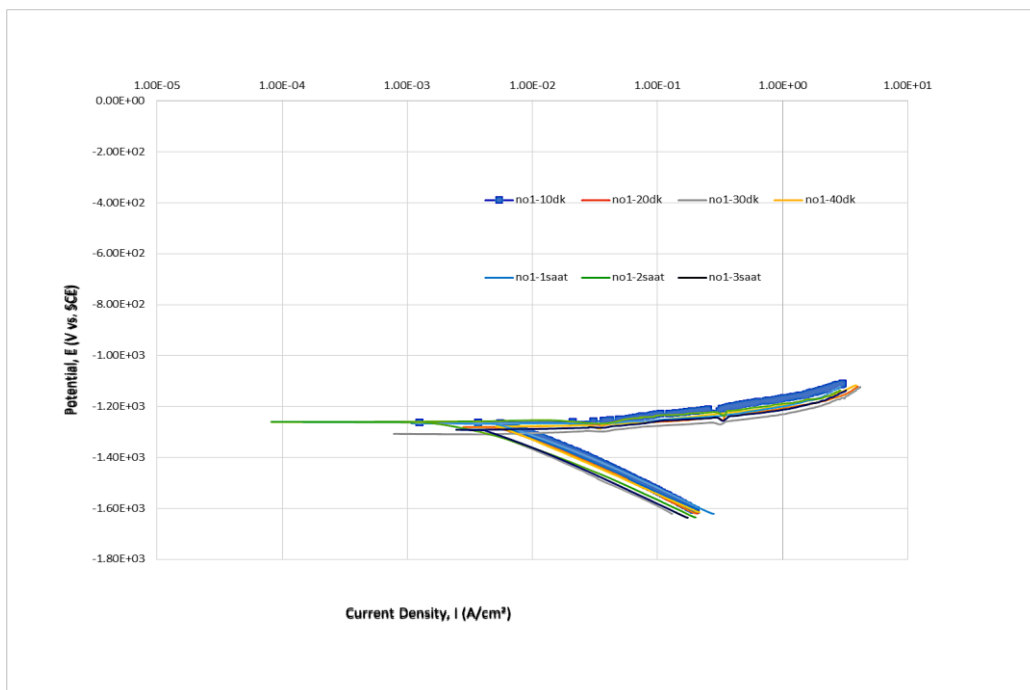


Figure 4.14. Potentiodynamic diagram for AZ31 samples in saline solution.

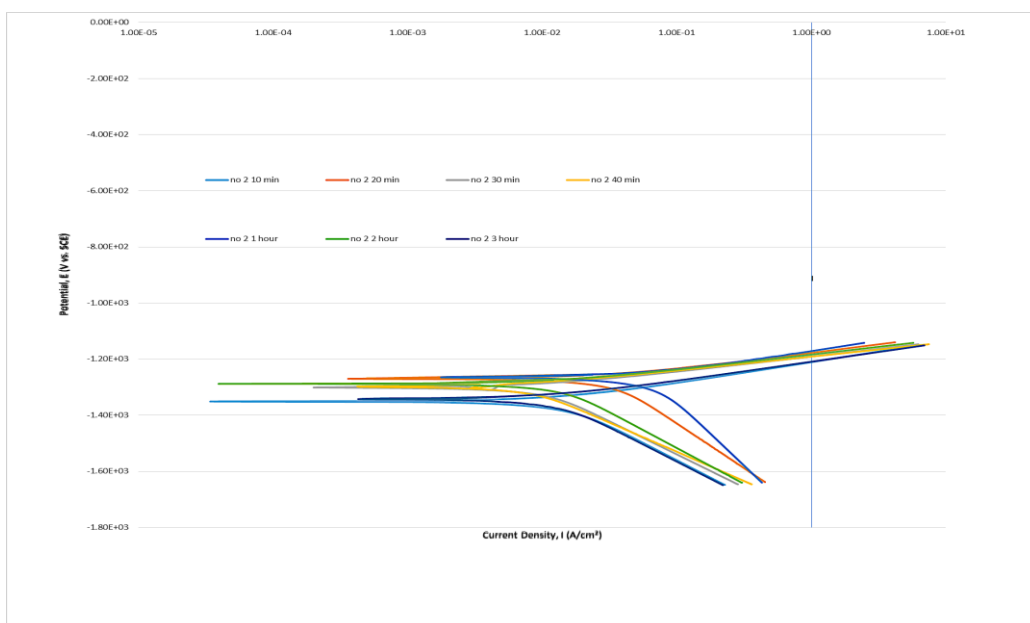


Figure 4.15. Potentiodynamic diagram for AZ31-0.5Nd-0.1 La samples in saline solution.

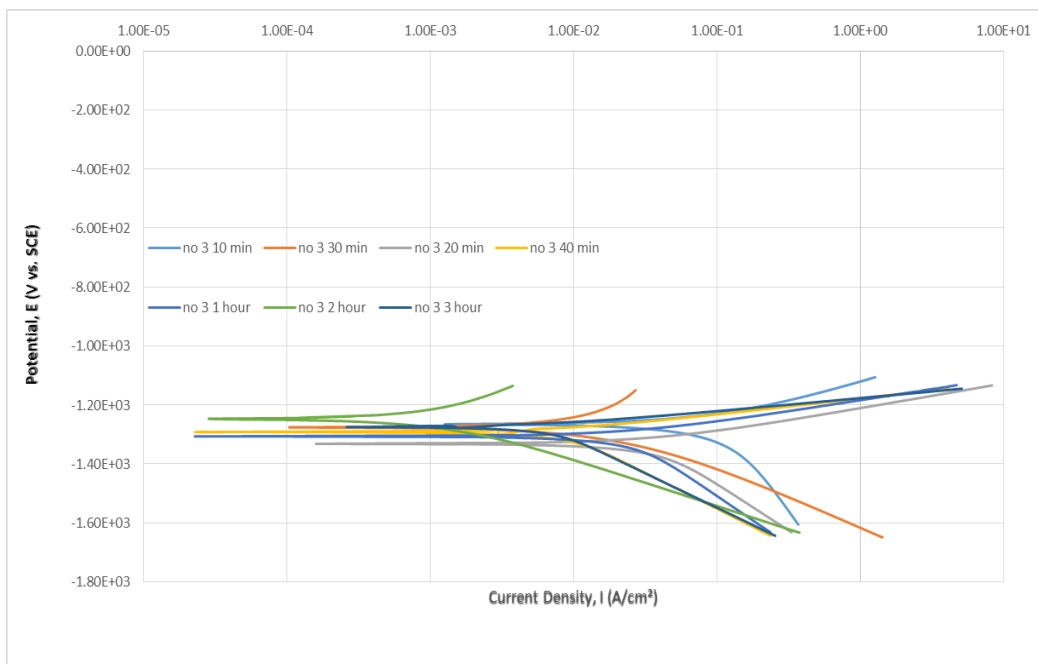


Figure 4.16. Potentiodynamic diagram for AZ31-0.5Nd-0.2 La samples in saline solution.

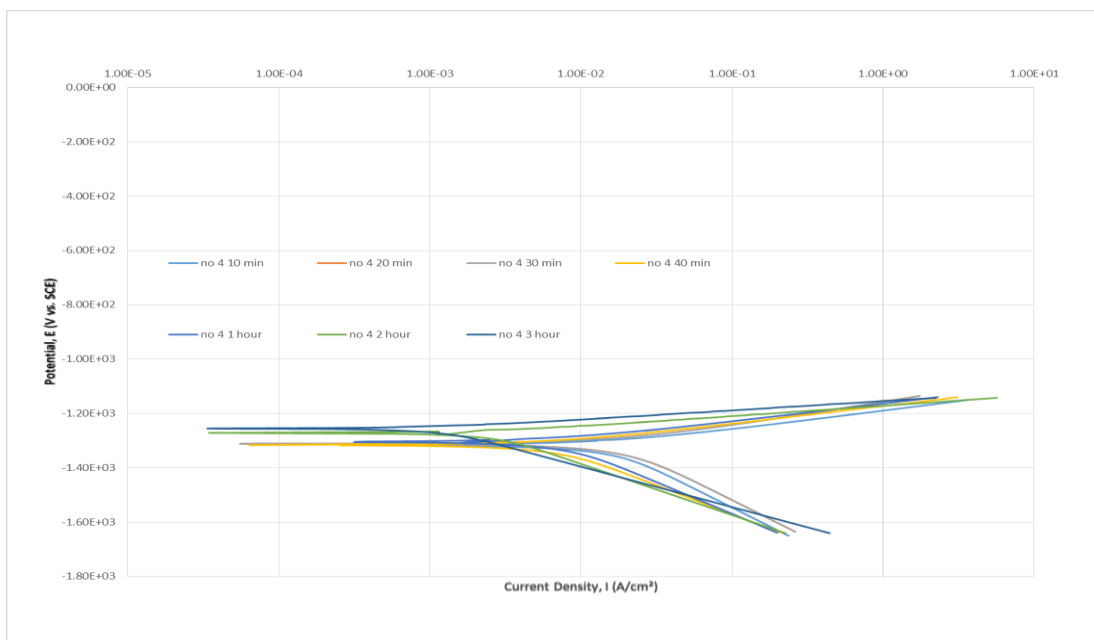


Figure 4.17. Potentiodynamic diagram for AZ31-0.5Nd-0.5 La samples in saline solution

Table 4.4. i_{corr} and E_{corr} rates for the corrosion test of the AZ31.

	Sample	$i_{corr}(\mu A/cm^2)$	E_{corr} (V)
AZ31	AZ31-10min	8.91	-1.260
	AZ31-20 min	8.59	-1.280
	AZ31-30 min	7.84	-1.310
	AZ31-40 min	8.38	-1.280
	AZ31-1h	7.71	-1.270
	AZ31-2h	3.19	-1.26
	AZ31-3h	6.36	-1.290
AZ31-0.5Nd-0.1 La	AZ31-0.5Nd-0.1 La -10 min	14.30	-1.35
	AZ31-0.5Nd-0.1 La -20 min	30.80	-1.27
	AZ31-0.5Nd-0.1 La -30 min	9.79	-1.3
	AZ31-0.5Nd-0.1 La -40 min	7.73	-1.3
	AZ31-0.5Nd-0.1 La -1h	64.50	-1.26
	AZ31-0.5Nd-0.1 La -2h	12.80	-1.29
	AZ31-0.5Nd-0.1 La -3h	12.20	-1.34
AZ31-0.5Nd-0.2 La	AZ31-0.5Nd-0.2 La -10 min	119.00	-1.27
	AZ31-0.5Nd-0.2 La	37.10	-1.33

AZ31-0.5Nd- 0.2 La	-20 min		
	AZ31-0.5Nd-0.2 La -30 min	25.90	-1.28
	AZ31-0.5Nd-0.2 La -40 min	8.60	-1.29
	AZ31-0.5Nd-0.2 La -1h	24.50	-1.31
	AZ31-0.5Nd-0.2 L-2h a	1.36	-1.25
	AZ31-0.5Nd-0.2 La -3h	6.73	-1.27
	AZ31-0.5Nd- 0.5 La	AZ31-0.5Nd-0.5 La -10 min	15.10
AZ31-0.5Nd-0.5 La -20 min		18.10	-1.31
AZ31-0.5Nd-0.5 La -30 min		7.42	-1.3
AZ31-0.5Nd-0.5 La -40 min		6.44	-1.32
AZ31-0.5Nd-0.5 La -1h		7.36	-1.3
AZ31-0.5Nd-0.5 La -2h		2.48	-1.27
AZ31-0.5Nd-0.5 La -3h		1.14	-1.26

It can be concluded from the figures from Figure 4.18 to Figure 4.21 and Table 4.4 that the corrosion is (the highest value at AZ31-0.5Nd-0.1 La-20 min and the lowest value AZ31- 2hour) when corrosion is in salt medium .

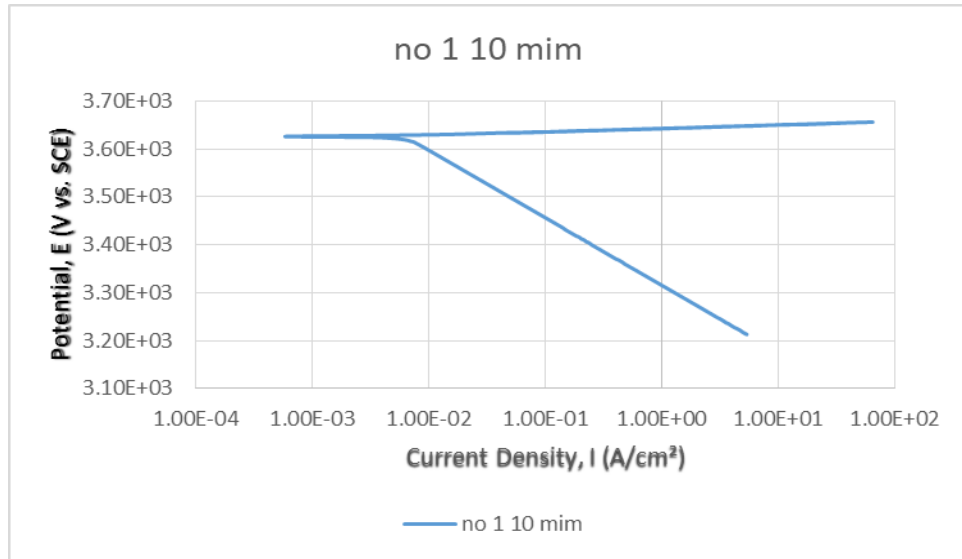


Figure 4.18. Potentiodynamic diagram of AZ31 samples in SBF.

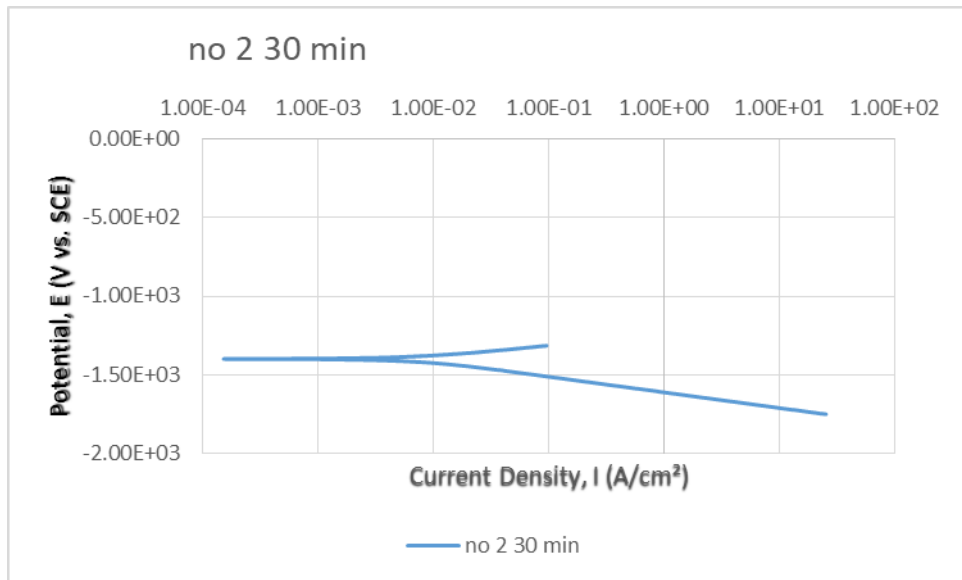


Figure 4.19. Potentiodynamic diagram of AZ31-0.5Nd-0.1 La samples in SBF.

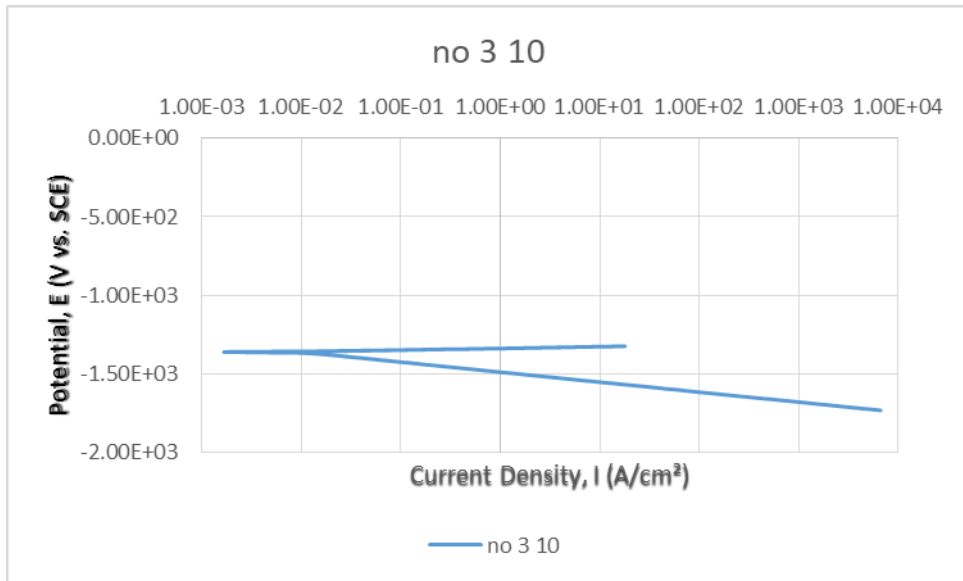


Figure 4.20 Potentiodynamic diagram of AZ31-0.5Nd-0.2 La samples in SBF.

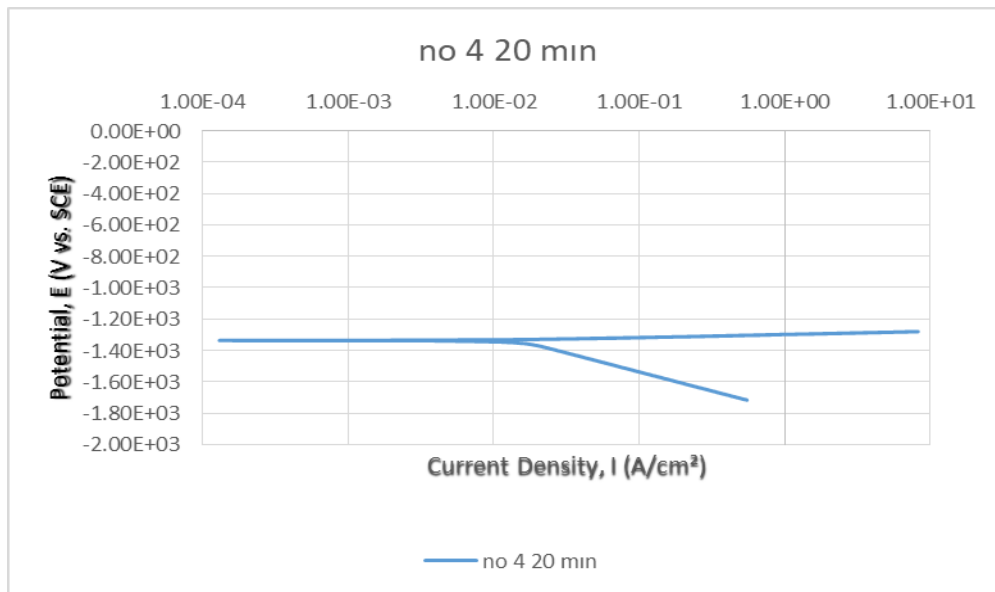


Figure 4.21. Potentiodynamic diagram of AZ31-0.5Nd-0.5 La samples in SBF.

Table 4.5. \dot{I}_{corr} and E_{corr} rates for the corrosion test of the AZ31 with SBF.

	Sample	$\dot{I}_{corr}(\mu A/cm^2)$	E_{corr} (V)
AZ31	AZ31-10 min	6.10	3.630
AZ31-0.5Nd-0.1 La	AZ31-0.5Nd-0.1 La -30min	7.34	-1.4
AZ31-0.5Nd-0.2 La	AZ31-0.5Nd-0.2 La -20min	9.77	-1.36
AZ31-0.5Nd-0.5 La	AZ31-0.5Nd-0.5 La -20min	14.90	-1.34

The results of the potentiodynamic polarization tests are given in Figs 4.14-4.21 as alloys containing only La and Mg Ag alloys containing additional alloying elements, respectively. The corrosion behavior of Mg alloys is mostly evaluated using initial corrosion rate measurements obtained by short-term methods (polarization curves or impedance measurements immediately after immersion of the sample in the electrolyte) . Therefore, having accurate and fast methods for the measurement of corrosion rates of alloys is of great importance for practical applications [78].

Corrosion of Mg-based implants results in four components: an abraded surface on the implant; dissolved Mg ions and other alloying elements; large amount of OH^- ; and hydrogen gas. SBF solutions used in in vitro studies contain large amounts of buffering agents such as HCO_3^- , HPO_4^{2-} , Tris HCl, and Hepes, which can deplete the OH^- produced and mediate sudden changes in pH . Therefore, although Mg dissolves quickly in these buffered solutions, the pH changes slowly [79]. In line with these

effects, the results of polarization and immersion tests on both Pure Mg and Mg Ag alloys have been reported.

It is concluded from the figures given in Fig. 5.1.1.5 to Fig. 5.1.1.8 and Table 5.1.1.2 that the corrosion is (highest value at AZ31-0.5Nd-0.5 La-20 minutes The lowest value is AZ31-10 min) when the corrosion is in a biological medium.

PART 5

CONCLUSIONS

In this study, the effect of heat treatment was studied by adding La and Nd to AZ31 alloys on the corrosion rate. Two types of corrosion were studied in POTENTIODYNAMIC CORROSION TEST and IMMERSION TEST. The microstructure was studied by OM microscope and SEM microscope. The elements were analyzed by EDX device. Wear test was carried out and the results were according to the following :

- i. Corrosion is (maximum value at AZ31-0.5Nd-0.1 La-20 min and minimum value AZ31-2 hours) when the corrosion occurs in a saline environment. Corrosion is maximum value at AZ31-0.5Nd-0.5 La-20 minutes The lowest value is AZ31-10 min) when corrosion occurs in a biological.
- ii. In the immersion test, AZ31-10 min shows the greatest weight loss and AZ31-0.5Nd-0.5 La-3h. has the lowest weight loss. In addition, 24-48 hours after the start of the dive, it was noted that the mass loss due to the formation of salts and dissolved elements in the dipping solution on the surface of the tested samples was less than the previous readings.
- iii. The optical microstructure images of the AZ31 alloy show that crystalline boundaries form in most samples and twinning is observed in some of the coarse grains of the alloys to which 0.5 Nd and %La% have been added. Due to the slow cooling process after heat treatment, the grain size is large.
- iv. In the SEM analysis, the grains of aluminum, zinc and manganese had a semicircular shape (semispongeous manganese) and the elements (La and Nd) added to the AZ31 alloy were in the form of short fibers. EDX analysis reveals the building blocks of each alloy.

- v. In the wear test, the wear rate in biological media was higher than that in the dry environment, where alloy AZ31-0.5 Nd-0.1 La-1hour recorded the highest wear rate in the wear test. AZ31 alloy and biological solution medium recorded the highest wear rate -0.5Nd-0.2 La-2hour in dry

REFERENCES

1. Hu, C., et al., “Bioinspired surface modification of orthopedic implants for bone tissue engineering”, *Biomaterials*,219: 119366 (2019).
2. Ibrahim, M.Z., et al., “Biomedical materials and techniques to improve the tribological, mechanical and biomedical properties of orthopedic implants–A review article”, *Journal of Alloys and Compounds*,714: 636-667 (2017).
3. Solanke, S., V. Gaval, and S. Sanghavi, “In vitro tribological investigation and osseointegration assessment for metallic orthopedic bioimplant materials”, *Materials Today: Proceedings*,44: 4173-4178 (2021).
4. Hamdaoui, S., et al., “An efficient and inexpensive method for functionalizing metallic biomaterials used in orthopedic applications”, *Colloid and Interface Science Communications*,37: 100282 (2020).
5. Staiger, M.P., et al., “Magnesium and its alloys as orthopedic biomaterials: a review”, *Biomaterials*,27(9): 1728-1734 (2006).
6. Esmaily, M., et al., “Fundamentals and advances in magnesium alloy corrosion”, *Progress in materials science*,89: 92-193 (2017).
7. Okuma, T., “Magnesium and bone strength”, *Nutrition (Burbank, Los Angeles County, Calif.)*,17(7-8): 679-680 (2001).
8. Yin, Z.-Z., et al., “Advances in coatings on biodegradable magnesium alloys”, *Journal of Magnesium and Alloys*,8(1): 42-65 (2020).
9. Liu, Y., “Corrosion Behaviour of Biodegradable Mg-1Ca Alloy in Simulated Body Fluid”. *The University of Manchester (United Kingdom)*(2018).
10. Ali, M., M. Hussein, and N. Al-Aqeeli, “Magnesium-based composites and alloys for medical applications: A review of mechanical and corrosion properties”, *Journal of Alloys and Compounds*,792: 1162-1190 (2019).
11. Hornberger, H., S. Virtanen, and A.R. Boccaccini, “Biomedical coatings on magnesium alloys–a review”, *Acta Biomaterialia*,8(7): 2442-2455 (2012).

12. Dong, H., et al., "Corrosion behavior of biodegradable metals in two different simulated physiological solutions: Comparison of Mg, Zn and Fe", *Corrosion Science*,182: 109278 (2021).
13. Ratner, B.D., et al., "Biomaterials science: an introduction to materials in medicine". *Elsevier*(2004).
14. Sumita, M., et al., "Failure processes in biometallic materials", *Comprehensive Structural Integrity*: 131-167 (2003).
15. Brooks, E.K., R.P. Brooks, and M.T. Ehrensberger, "Effects of simulated inflammation on the corrosion of 316L stainless steel", *Materials Science and Engineering: C*,71: 200-205 (2017).
16. Marques, A., R. Reis, and J. Hunt, "The biocompatibility of novel starch-based polymers and composites: in vitro studies", *Biomaterials*,23(6): 1471-1478 (2002).
17. Dos Santos, V., R.N. Brandalise, and M. Savaris, "Engineering of biomaterials". *Springer*.10. (2017).
18. Chowdhury, S.K., V. Nagarjuna, and B. Bhaskar, "Metallic Biomaterials in Tissue Engineering: Retrospect and Prospects", *Biomaterials in Tissue Engineering and Regenerative Medicine: From Basic Concepts to State of the Art Approaches*: 19-60 (2021).
19. Friedrich, H.E. and B.L. Mordike, "Magnesium technology". *Springer*.212. (2006).
20. Kirkland, N., N. Birbilis, and M. Staiger, "Assessing the corrosion of biodegradable magnesium implants: A critical review of current methodologies and their limitations", *Acta Biomaterialia*,8(3): 925-936 (2012).
21. Poinern, G.E.J., S. Brundavanam, and D. Fawcett, "Biomedical magnesium alloys: a review of material properties, surface modifications and potential as a biodegradable orthopaedic implant", *American Journal of Biomedical Engineering*,2(6): 218-240 (2012).
22. Agarwal, S., et al., "Biodegradable magnesium alloys for orthopaedic applications: A review on corrosion, biocompatibility and surface modifications", *Materials Science and Engineering: C*,68: 948-963 (2016).

23. Russell, A. and W. Hugo, “7 antimicrobial activity and action of silver”, *Progress in medicinal chemistry*,31: 351-370 (1994).
24. Wells, T.N., et al., “Mechanism of irreversible inactivation of phosphomannose isomerases by silver ions and flomoxone”, *Biochemistry*,34(24): 7896-7903 (1995).
25. Thurman, R.B., C.P. Gerba, and G. Bitton, “The molecular mechanisms of copper and silver ion disinfection of bacteria and viruses”, *Critical reviews in environmental science and technology*,18(4): 295-315 (1989).
26. Witte, F., et al., “Degradable biomaterials based on magnesium corrosion”, *Current opinion in solid state and materials science*,12(5-6): 63-72 (2008).
27. Gu, X., et al., “In vitro corrosion and biocompatibility of binary magnesium alloys”, *Biomaterials*,30(4): 484-498 (2009).
28. Gupta, M. and S.N.M. Ling, “Magnesium, magnesium alloys, and magnesium composites”. *John Wiley & Sons*(2011).
29. Hirsch, J., B. Skrotzki, and G. Gottstein, “Aluminium alloys: the physical and mechanical properties”. *John Wiley & Sons*.1. (2008).
30. Mezbahul-Islam, M., A. Mostafa, and M. Medraj, “Essential magnesium alloys binary phase diagrams and their thermochemical data”, *Journal of Materials*,2014 (2014).
31. Raynor, G.V. and R. Smith, “The transition temperature of the transition between grey and white tin”, *Proceedings of the Royal Society of London. Series A. Mathematical and Physical Sciences*,244(1236): 101-109 (1958).
32. Sundgren, J.-E., “Structure and properties of TiN coatings”, *Thin solid films*,128(1-2): 21-44 (1985).
33. Dev, A., et al., “A systematic investigation of secondary phase dissolution in Mg–Sn alloys”, *Journal of Magnesium and Alloys*,7(4): 725-737 (2019).
34. Lynch, R., “Zinc: alloying, thermomechanical processing, properties, and applications”, *Encyclopedia of Materials: Science and Technology*: 9869-9883 (2001).
35. Rollez, D., A. Pola, and F. Prenger, “Zinc alloy family for foundry purposes”, *WORLD OF METALLURGY, ERZMETALL*,68(6): 354-358 (2015).
36. Baker, H., “Alloy phase diagrams”, *ASM handbook*,3: 2-80 (1992).

37. Dan’Kov, S.Y., et al., “Magnetic phase transitions and the magnetothermal properties of gadolinium”, *Physical Review B*,57(6): 3478 (1998).
38. Blawert, C., N. Hort, and K. Kainer, “Automotive applications of magnesium and its alloys”, *Trans. Indian Inst. Met*,57(4): 397-408 (2004).
39. Tekumalla, S., et al., “Mechanical properties of magnesium-rare earth alloy systems: A review”, *Metals*,5(1): 1-39 (2014).
40. Hort, N., et al., “Magnesium alloys as implant materials–Principles of property design for Mg–RE alloys”, *Acta Biomaterialia*,6(5): 1714-1725 (2010).
41. Wang, B., et al., “Production of Fe–Ti alloys from mixed slag containing titanium and Fe₂O₃ via direct electrochemical reduction in molten calcium chloride”, *Metals*,10(12): 1611 (2020).
42. Peron, M., F. Berto, and J. Torgersen, “Magnesium and Its Alloys as Implant Materials: Corrosion, Mechanical and Biological Performances”. *CRC Press*(2020).
43. Gong, H., et al. “*Micro characterization of Mg and Mg alloy for biodegradable orthopedic implants application*”. in *International Manufacturing Science and Engineering Conference*. American Society of Mechanical Engineers (2012).
44. Putra, A.G., A. Manaf, and A. Anawati. “*Enhancing the Hardness of Mg-9Al-1Zn Cast Alloy by Solution Treatment*”. in *IOP Conference Series: Materials Science and Engineering*. IOP Publishing (2019).
45. Schinhammer, M., et al., “Design strategy for biodegradable Fe-based alloys for medical applications”, *Acta Biomaterialia*,6(5): 1705-1713 (2010).
46. Cecchinato, F., et al., “Influence of magnesium alloy degradation on undifferentiated human cells”, *PloS one*,10(11): e0142117 (2015).
47. Polmear, I., “Light alloys: from traditional alloys to nanocrystals”. *Elsevier*(2005).
48. Kainer, K.U. and B.L. Mordike, “Magnesium alloys and their applications”. *Wiley-Vch Weinheim*(2000).
49. Freitas, R.A., “Nanomedicine, volume I: basic capabilities”. *Landes Bioscience Georgetown, TX*.1. (1999).
50. Munoz, A.I., N. Espallargas, and S. Mischler, “Tribocorrosion”. *Springer*(2020).

51. Carboneras, M., M. García-Alonso, and M. Escudero, "Biodegradation kinetics of modified magnesium-based materials in cell culture medium", *Corrosion Science*,53(4): 1433-1439 (2011).
52. Witte, F., et al., "In vivo corrosion of four magnesium alloys and the associated bone response", *Biomaterials*,26(17): 3557-3563 (2005).
53. Stansbury, E.E. and R.A. Buchanan, "Fundamentals of electrochemical corrosion". *ASM international*(2000).
54. Makar, G. and J. Kruger, "Corrosion of magnesium", *International materials reviews*,38(3): 138-153 (1993).
55. Song, Y., et al., "The role of second phases in the corrosion behavior of Mg–5Zn alloy", *Corrosion Science*,60: 238-245 (2012).
56. AL-GBURI, A.S.N., *THE INVESTIGATION OF BIODEGRADABLE CORROSION PROPERTIES OF HOT ROLLED AT31 MG ALLOYS*. 2022.
57. Song, G.L. and A. Atrens, "Corrosion mechanisms of magnesium alloys", *Advanced Engineering Materials*,1(1): 11-33 (1999).
58. Mankins, W. and S. Lamb, "Nickel and nickel alloys", (1990).
59. Incesu, A. and A. Gungor, "Mechanical properties and biodegradability of Mg–Zn–Ca alloys: homogenization heat treatment and hot rolling", *Journal of Materials Science: Materials in Medicine*,31: 1-12 (2020).
60. Brady, M., et al., "Film breakdown and nano-porous Mg (OH) 2 formation from corrosion of magnesium alloys in salt solutions", *journal of the Electrochemical Society*,162(4): C140 (2015).
61. Nordlien, J.H., et al., "Morphology and structure of oxide films formed on MgAl alloys by exposure to air and water", *journal of the Electrochemical Society*,143(8): 2564 (1996).
62. Lunder, O., T.K. Aune, and K. Nisancioglu, "Effect of Mn additions on the corrosion behavior of mould-cast magnesium ASTM AZ91", *Corrosion*,43(5): 291-295 (1987).
63. Song, G.-L., "Corrosion of magnesium alloys". *Elsevier*(2011).
64. Landolt, D., S. Mischler, and M. Stemp, "Electrochemical methods in tribocorrosion: a critical appraisal", *Electrochimica acta*,46(24-25): 3913-3929 (2001).

65. Cao, S. and S. Mischler, "Modeling tribocorrosion of passive metals—A review", *Current opinion in solid state and materials science*,22(4): 127-141 (2018).
66. Yan, Y., "Bio-tribocorrosion in biomaterials and medical implants". *Elsevier*(2013).
67. Kajdas, C. and K.i. Hiratsuka, "Tribocatalysis, Tribochemistry, and Tribocorrosion". *CRC Press*(2018).
68. Watson, S., et al., "Methods of measuring wear-corrosion synergism", *Wear*,181: 476-484 (1995).
69. Bhargava, A. and M. Banerjee, "2.14 Heat-Treating Copper and Nickel Alloys", (2017).
70. Mallick, P.K., "Materials, design and manufacturing for lightweight vehicles". *Woodhead publishing*(2020).
71. Soltan, A.A., et al., "Examination of the Corrosion Behavior of Shape Memory NiTi Material for Biomedical Applications", *Materials*,16(11): 3951 (2023).
72. Zhang, J., et al., "Microstructures and mechanical properties of heat-resistant high-pressure die-cast Mg–4Al–xLa–0.3 Mn (x= 1, 2, 4, 6) alloys", *Materials science and Engineering: A*,527(10-11): 2527-2537 (2010).
73. Kumar, A., et al., "Lanthanum effect on improving CTE, damping, hardness and tensile response of Mg-3Al alloy", *Journal of Alloys and Compounds*,695: 3612-3620 (2017).
74. Liangming, Y., et al., "Effect of Homogenization on Microstructure and Mechanical Property of Mg-5.9 Zn-1.6 Zr-1.6 Nd-0.9 Y Alloy", *Rare Metal Materials and Engineering*,47(5): 1393-1398 (2018).
75. Du, Y., et al., "Effect of La addition on the microstructure and mechanical properties of Mg–6 wt% Zn alloys", *Materials science and Engineering: A*,673: 47-54 (2016).
76. Li, H., et al., "The influence of Zn content on the corrosion and wear performance of Mg-Zn-Ca alloy in simulated body fluid", *Journal of Materials Engineering and Performance*,25: 3890-3895 (2016).
77. Liu, D.-B., et al., "Corrosion and wear behavior of an Mg–2Zn–0.2 Mn alloy in simulated body fluid", *Rare Metals*,34: 553-559 (2015).

78. Feliu Jr, S., “Electrochemical impedance spectroscopy for the measurement of the corrosion rate of magnesium alloys: Brief review and challenges”, *Metals*,10(6): 775 (2020).
79. Xin, Y., T. Hu, and P. Chu, “In vitro studies of biomedical magnesium alloys in a simulated physiological environment: a review”, *Acta Biomaterialia*,7(4): 1452-1459 (2011).

RESUME

Sarah Khazaal Jabbar MADHI is a material engineer who graduated from the Production Engineering and Metallurgy/Metallurgy Engineering Engineering, University of Technology - Iraq. She received her Bachelor's degree in 2012/2013. she is currently studying for her Master's degree at Karabük University in the field of Materials Engineering.